Multifactorial SARS-CoV-2 seroprofiling dissects interdependencies with human coronaviruses and predicts neutralization activity

Irene A. Abela[1,2*], Chloé Pasin[1,2*], Magdalena Schwarzmüller[1*], Selina Epp[1], Michèle E. Sickmann[1], Merle M. Schanz[1], Peter Rusert[1], Jacqueline Weber[1], Stefan Schmutz[1], Annette Audigé[1], Liridona Maliqi[1], Annika Hunziker[1], Maria C. Hesselman[1], Cyrille R. Niklaus[1], Jochen Gottschalk[3], Eméry Schindler[3], Alexander Wepf[4], Urs Karrer[5], Aline Wolfensberger[2], Silvana K. Rampini[6], Patrick M. Meyer Sauteur[7], Christoph Berger[7], Michael Huber[1], Jürg Böni[1], Dominique L. Braun[1,2], Maddalena Marconato[8], Markus G. Manz[8], Beat M. Frey[3], Huldrych F. Günthard[1,2$], Roger D. Kouyos[1,2$], Alexandra Trkola[1$]

* shared authorship

[$] shared corresponding authors

Affiliations

[1] Institute of Medical Virology, University of Zurich, Switzerland

[2] Division of Infectious Diseases and Hospital Epidemiology, University Hospital Zurich, Switzerland

[3] Blood Transfusion Service Zurich, Switzerland

[4] Institute of Laboratory Medicine, Cantonal Hospital Winterthur, Switzerland

[5] Department of Medicine, Cantonal Hospital Winterthur, Switzerland

[6] Department of Internal Medicine, University Hospital Zurich, Switzerland

22 [7] Division of Infectious Diseases and Hospital Epidemiology, University Children's Hospital Zurich,
23 Switzerland

24 [8] Department of Medical Oncology and Hematology, University Hospital and University of Zurich,
25 Switzerland

26

27

Abstract

Definition of SARS-CoV-2 antibody responses is essential to verify protective immunity following infection and vaccination. Here, we devised a versatile serological test, named ABCORA, that is based on a multifactorial analysis of SARS-CoV-2 and circulating human coronavirus (HCoV) antibody responses. Utilizing empirical tailored cut-offs and computational approaches based on training and validation cohorts comprising pre-pandemic (N=825) and SARS-CoV-2 infected plasma donors (N=389), we defined several analysis strategies that allow a highly accurate definition of SARS-CoV-2 seroconversion and prediction of neutralization activity. Intriguingly, HCoV reactivity was significantly higher in SARS-CoV-2 negative donors. Amongst SARS-CoV-2 infected individuals, elevated SARS-CoV-2 responses were linked to higher HCoV activity suggesting that pre-existing HCoV immunity may confer protection against SARS-CoV-2 acquisition and promote development of SARS-CoV-2 specific antibody responses. Deciphering interdependencies between SARS-CoV-2 and HCoV immunity should be enforced as understanding their impact on infection may allow soliciting cross-protective activities for broader coronavirus prevention.

45 **Introduction**

46 Monitoring the antibody response to SARS-CoV-2 is critical to define correlates of vaccine protection,
47 differences in susceptibility to infection and in disease severity. The picture of the antibody landscape
48 to SARS-CoV-2 that has thus far evolved is complex. The antibody response to SARS-CoV-2 is rapid, and
49 triggers strong IgM, IgA and IgG responses [1,2]. Both binding and neutralizing responses increase with
50 disease severity and show in part dependence on demographic parameters such as age and gender [3-
51 5]. It remains, however, unclear which factors are independent drivers of antibody responses, reflect
52 severe disease courses or are confounded by other factors including infection length and co-
53 morbidities. Waning IgG binding and neutralizing antibody titers have been described in some but not
54 all convalescent cohorts and may be particularly pronounced in individuals with asymptomatic or mild
55 infection [6-9]. IgG responses to spike (S) glycoprotein may persist longer than to nucleocapsid protein
56 (N)[7,10,11] and can in part undergo affinity maturation post virus clearance [5]. Current serological analyses
57 predominantly focus on measuring reactivity to N, the spike glycoprotein S1 subunit and the ACE2
58 receptor-binding domain (RBD) in S1 [2,5,12-16]. Antibodies to RBD and the receptor-binding motif within
59 the RBD constitute the main group of neutralizing antibodies, followed by S1 trimer specific, spike N-
60 terminal domain, and spike S2 neutralizing antibodies [16-22]. S1 and RBD binding correlate with
61 neutralizing activity in both natural and vaccine-induced immune responses providing means to
62 estimate the potential for neutralization where neutralization capacity cannot be assessed directly [6,8].
63 Considering the complex antibody response patterns, possibilities to capture the dynamics of the
64 SARS-CoV-2 response across diverse Immunoglobulin (Ig) classes and SARS-CoV-2 antigens are needed
65 to ascertain sensitive detection of seroconversion and sero-reversion and to establish links to
66 protective, neutralizing activity.

67 Infections with circulating human coronaviruses (HCoV), alphacoronavirus (HCoV-229E, HCoV-NL63)
68 and betacoronavirus (HCoV-HKU1, HCoV-OC43), are common and contribute considerably to the
69 seasonal respiratory disease burden in humans [23,24]. Despite an overall modest sequence homology
70 between SARS-CoV-2 and circulating HCoVs, several conserved regions exist and antibody cross-

71 reactivity may occur [25-27]. While dismissed in the diagnostic setting as false-positives [28], cross-reactive
72 antibodies may bear biological relevance as suggested for S2 cross-neutralizing antibodies [29].
73 Uncertainty remains, however, whether cross-reactive HCoV antibody responses influence the
74 evolution of SARS-CoV-2 specific immunity. Positive impact by providing early low affinity memory
75 responses to build on and mature as well as negative influences following the antigenic sin principle [30]
76 by boosting non-protective cross-reactive antibodies on the expense of de-novo responses can be
77 envisaged. In view of this, the definition of pre-existing immunity due to prior infection with HCoVs
78 will remain complex in clinical diagnosis and strategies to record HCoV and SARS-CoV-2 responses side
79 by side are needed to fill this knowledge gap.

80 Here we report on the development of a serological assay that allows multifactorial seroprofiling of
81 SARS-CoV-2 and HCoV responses at high diagnostic accuracy. Seroprofiling of a large cohort of SARS-
82 CoV-2 infected and uninfected individuals provided key insights into the interdependencies of HCoV
83 and SARS-CoV-2 antibody responses. The results highlight a potential protective role of HCoV-specific
84 antibodies in SARS-CoV-2 acquisition as well as in shaping the SARS-CoV-2 response upon infection.

85

86

87 **Results**

88 **Multifactorial seroprofiling defines SARS-CoV-2 specific responses**

89 Recognizing the need for comprehensive SARS-CoV-2 serological profiling to elucidate central
90 questions in SARS-CoV-2 immunity and its interdependencies with HCoV responses, we created a bead-
91 based multiplex immunoassay using the Luminex technology© to measure specific IgG, IgA and IgM
92 responses to SARS-CoV-2 RBD, S1, S2 and N (Supplementary Fig. 1). The assay records in total 12 SARS-
93 CoV-2 specific antibody parameters (4 antigens across 3 Ig classes) with high diagnostic accuracy (see
94 methods, Supplementary Fig. 1-4 and Supplementary Tables 1, 2) and further includes the S1 protein
95 of HCoV-HKU1 to screen cross-reactive antibodies alongside SARS-CoV-2 responses. According to the
96 test's design to monitor antibodies to two coronaviruses, we termed the assay **A**nti**b**ody **COR**onavirus
97 **A**ssay (ABCORA) 2.0.
98 Measurements in ABCORA are expressed as median fluorescence intensity (MFI) corrected for
99 background binding (fold over empty beads, FOE). To distinguish SARS-CoV-2-specific from cross-
100 reactive antibodies, we defined MFI-FOE thresholds for each of the 12 SARS-CoV-2 antigen and Ig class
101 combinations based on plasma antibody reactivity in training cohorts of pre-pandemic healthy donor
102 plasma (Training I, N=573) and in donors with confirmed SARS-CoV-2 infection (Training III, N=175)
103 (Fig. 1a, Supplementary Table 3). Thresholds were set to minimize false-positives while ensuring
104 sensitivity for SARS-CoV-2 antibody detection (Fig. 1a, c, Supplementary Table 3). Signal over cut-off
105 (SOC) values were calculated for each of the 12 SARS-CoV-2 antibody parameters based on the
106 established threshold values. Positive call criteria were defined to ascertain that in at least two of the
107 12 antigen and Ig combinations the threshold is reached (Supplementary Table 4). The final threshold
108 and positive call criteria allowed for a differentiation of partial (only IgM and IgA responses) to full
109 seroconversion (including IgG responses). In addition, the criteria denote samples with weak reactivity
110 and/or indeterminate reactivity (Supplementary Table 5).

111 We further evaluated the ABCORA 2.0 test in clinical samples of pre-pandemic patients with
112 documented, recent HCoV infection (Training II, N= 75, OC43 (N=27), HKU1 (N=17), NL63 (N=22), 229E
113 (N=9)). This group comprised individuals with different underlying severe diseases including immune
114 compromised patients that underwent diagnostic screening for HCoV. We noted an overall lower
115 reactivity with SARS-CoV-2 in this syndromic group but importantly observed no indication of cross-
116 reactivity that affects the ABCORA readout. (Fig. 1a, b). Considering data of all training cohorts (I-III),
117 ABCORA 2.0 exhibited a high sensitivity and specificity, reaching 94.29% sensitivity and 99.07%
118 specificity (Fig. 1c, Supplementary Table 3).

119 To obtain insight into potential cross-reactivity with HCoV antibodies, we recorded reactivity to the S1
120 unit of HCoV-HKU1 in addition to the SARS-COV-2 antigens (Fig. 1a). Owing to the high prevalence of
121 HCoV antibodies and the ensuing lack of true-negative controls, we set no thresholds to rate HKU1
122 reactivity as positive/negative. Overall, SARS-CoV-2 cross-reactivity was low in pre-pandemic samples
123 despite notable HKU1 activity (Fig. 1a). Correlation analysis of SARS-CoV-2 and HKU1 plasma antibody
124 reactivity in SARS-CoV-2 positive donors indicated no correlation in IgG but a substantial cross-
125 reactivity between HKU1 S1 IgM and to lesser extent also IgA (Supplementary Fig. 5a). In pre-pandemic
126 individuals, IgM binding to SARS-CoV-2 and HKU1 was highly correlated whereas IgG and IgA
127 reactivities were less affected (Supplementary Fig. 5b). Of note, individuals with recent HCoV infection
128 showed the highest correlation in IgM between HKU1 and SARS-CoV-2 (Supplementary Fig. 5d). These
129 data underline that cross-reactivity needs to be considered but mostly affects low level responses as
130 evidenced by the measurements in pre-pandemic individuals (Fig. 1a, b, Supplementary Fig. 5).

131 We verified the performance of ABCORA 2.0 on separate validation cohorts of pre-pandemic healthy
132 adults (N=252), pre-pandemic children (N=169) and individuals with documented SARS-CoV-2 infection
133 (N= 214) (Fig. 1 a, b, Supplementary Table 3). The outcome of this assessment confirmed the validity
134 of the chosen assay criteria. Sensitivity and specificity of the combined negative cohorts were even
135 slightly higher than in the training cohort (Fig. 1c). Of note, when analyzing children and adults in the
136 validation cohort separately, we observed a slightly lower specificity amongst children (98.82%)

137 compared to adults (99.60%), raising the possibility that cross-reactive activity in children may be more
138 prevalent than in adults (Fig. 1a). Indeed, pre-pandemic children showed a higher correlation of IgM
139 HKU1 and SARS-CoV-2 (Supplementary Fig. 5c), highlighting that interpretation of IgM SARS-CoV-2
140 activity can be complex. Importantly, combining training and validation cohorts of SARS-CoV-2 positive
141 individuals (N=389) and negative controls (N= 825), ABCORA 2.0 achieved a sensitivity of 94.60% and
142 a specificity of 99.16%, underlining the high capacity of the test in accurately assessing SARS-CoV-2
143 seropositivity (Fig. 1c).

144

145 **Computational analyses maximize specificity and sensitivity of SARS-CoV-2 seroprofiling**

146 We next sought to devise computational analysis extensions to further increase specificity. We
147 compared two analysis approaches, the first was based on a logistic regression model (ABCORA 2.1),
148 the second on a random forest model (ABCORA 2.2). Instead of obtaining 12 individual thresholds (one
149 per antigen and Ig class) as in ABCORA 2.0, both computational models solely estimate the probability
150 of a sample to be positive by providing a composite result across all 12 measurements and ranking sera
151 positive or negative (1, 0 classification). Both analysis strategies were established on the training
152 dataset used for the setup of ABCORA 2.0 (Training I–III, Fig. 1). For the logistic regression ABCORA 2.1,
153 we grouped SARS-CoV-2 binding activities displaying high correlation (Supplementary Fig. 6a) and
154 included the mean value of their MFI-FOEs in the model. The analysis on the validation data sets
155 recorded 93.46% sensitivity and 99.60% specificity in adults and 99.41% specificity in children. When
156 assessed with the combined training and validation cohort data sets, 93.57% sensitivity and 99.35%
157 specificity were detected (Fig. 1c, Supplementary Table 3).

158 The random forest model ABCORA 2.2 included all 12 SARS-CoV-2 responses measured and aggregated
159 the result of 1000 classification trees. ABCORA 2.2 succeeded in tailoring thresholds tightly to the
160 training data sets, obtaining classification settings with 100% specificity and 100% sensitivity. This high
161 specificity was confirmed by analysis of the validation data sets (IV and V) comprising pre-pandemic

162 samples from healthy adults (specificity 100%) and children (specificity 99.41%). ABCORA 2.2 reached
163 a sensitivity of 95.33% in the validation set, outperforming both ABCORA 2.0 and 2.1. Of note, positive
164 calling by ABCORA 2.2 was dominated by IgG responses (Supplementary Fig. 6b). On the combined
165 training and validation cohorts of SARS-CoV-2 positive individuals (N=389) and negative controls (N=
166 825), ABCORA 2.2 achieved a striking sensitivity of 97.43% and a specificity of 99.91%. Prompted by
167 the observed correlation between SARS-CoV-2 and HKU1 IgM and to a lesser extent IgA responses, we
168 next explored whether incorporation of HKU1 reactivity into the random forest model may further
169 improve the calling specificity and sensitivity. Indeed, a model that included HKU1 S1 as additional
170 variable (ABCORA 2.3) increased sensitivity from 97.43% in ABCORA 2.2 to 98.20% (Fig. 1c,
171 Supplementary Table 3) without reduction of the specificity. Owing to its combined high sensitivity and
172 specificity, we therefore selected ABCORA 2.3 as the analysis strategy for rating global SARS-CoV-2
173 seroconversion.

174 We next verified the accuracy of ABCORA 2.0 and 2.3 in defining positive and negative SARS-CoV-2
175 immune status utilizing the National Institute for Biological Standards and Control (NIBSC) Anti SARS-
176 CoV-2 Verification Panel (20/B770)[31]. This verification panel for serology assays includes 23 positive
177 and 14 negative serum samples and allows direct comparison with other test systems [31]. Both ABCORA
178 versions showed 100% sensitivity and 100% specificity on the verification plasma panel and compared
179 favorably to commercial assay systems (Fig. 1d, Supplementary Table 6). To cross-reference these
180 external verification results, we next compared the sensitivity of the ABCORA tests and three
181 commercial serology test systems on a subset of the SARS-CoV-2 positive training cohort (cohort III,
182 N=171) for which sufficient material remained. Assays targeting the N protein (Elecsys® Anti-SARS-
183 CoV-2 (Roche Diagnostics GmbH)), the RBD region of the S protein (Elecsys® Anti-SARS-CoV-2 S assay
184 (Roche Diagnostics GmbH)), and the S1 subunit (EUROIMMUN Anti-SARS-CoV-2 ELISA (IgG)) were
185 included. The results confirmed the analysis on the international NIBSC 20/B770 plasma panel, with
186 ABCORA 2.0 and ABCORA 2.3 showing the highest sensitivity amongst the tested assays
187 (Supplementary Table 7).

188 We thus conclude that ABCORA 2.0 seroprofiling in combination with ABCORA 2.3 defines positivity
189 with the highest specificity and sensitivity. The individual antigen response evaluation by ABCORA 2.0
190 defines the stage of seroconversion status based on individual IgM, IgA and IgG cut-off values and
191 thereby complements and maximizes the information that can be obtained by ABCORA 2 seroprofiling.

192

193 **Predicting SARS-CoV-2 neutralization based on ABCORA seroprofiling**

194 Determining neutralization activity is critical to gauge protective immunity. While neutralization can
195 be directly measured with a range of authentic virus or pseudovirus SARS-CoV-2 neutralization tests
196 [5,22,32], applying direct binding or competition tests as surrogate for neutralization activity remains of
197 high interest as these test systems are faster, less labor-intensive, widely applicable and scalable [32,33].
198 In particular, S1 and RBD binding has been shown to correlate well with neutralization activity [5,8,19,32-
199 36]. To explore neutralization predictors based on ABCORA 2.0, we probed in a first step the capacity of
200 ABCORA to derive quantitative S1 and RBD readouts in a subset of SARS-CoV-2 positive patients (N=72).
201 ABCORA 2.0 measurements of serially diluted plasma were conducted to derive 50% effective
202 concentrations (EC50, expressed as reciprocal plasma dilution) and area under the curve values (AUC
203 expressed as MFI) for all 12 SARS-CoV-2 parameters (Fig. 2a, b). In addition, we quantified SARS-CoV-
204 2 RBD and S1 responses via the RBD specific mAb CR3022 [37] (Fig. 2c) and the WHO International
205 Standard Anti-SARS-CoV-2 Immunoglobulin NIBSC 20/136[31] (Supplementary Fig. 7b, Supplementary
206 Table 8). For this we quantified the respective antibody content of a positive control SARS-CoV-2 donor
207 pool included in all ABCORA measurements and expressed the antibody content of individual plasma
208 samples in relation to it (Fig. 2c, Supplementary Fig. 7). We then probed which of the ABCORA
209 quantitative readouts correlated best with each other, the basic readout of ABCORA 2.0 (MFI-FOE at
210 plasma dilution 1/100), and the quantitative Roche Elecsys S test (U/ml) (Fig. 2c, Supplementary Fig.
211 7). In addition to the individual antigen parameters, we also considered cumulative response values.
212 These were total spike reactivity (sum of RBD, S1, S2 across all Ig classes), Ig class spike reactivity (sum
213 of S1, RBD, S2 for one isotype) and antigen specific reactivity (sum of all Ig classes for one antigen). We

214 observed a genuinely good correlation across the diverse spike parameters tested (Fig. 2d). The
215 notable exception were classical EC50 values, which showed no to weak correlation across all
216 parameters including the commercial test. Interestingly, AUC values, which in contrast to EC50 are a
217 composite measure of concentration and signal strength, performed well. Of note, we observed highly
218 variable SARS-CoV-2 antibody dose response curves, reaching in our cohort individual plateaus over a
219 4-log range (Supplementary Fig. 7). These plateaus are respected in the AUC readout, and are also
220 recorded by the basic MFI-FOE ABCORA readout at 1/100 plasma dilution, but are not considered in
221 EC50 determinations. Indeed the basic MFI-FOE showed a high correlation with the quantitative
222 readouts across the tested variables including the quantitative commercial Roche Elecsys S test.

223 Based on these results, we concluded that the MFI-FOE readout at 1/100 provides an excellent
224 estimate for the S1 and RBD antibody content in plasma and that this straightforward and easily
225 obtainable readout, which only requires a single plasma dilution to be tested, can be used as a proxy
226 for quantification. We therefore employed the basic MFI-FOE in a next step to define neutralization
227 predictors.

228 Neutralization activity to Wuhan-Hu-1 in SARS-CoV-2 positive individuals (N=467) using an established
229 SARS-CoV-2 pseudovirus neutralization test [5,22,32] revealed a broad range of 50% neutralizing titers
230 (NT50) (post positive RT-PCR Fig. 3a (N=369), post onset of symptoms, Supplementary Fig. 8a (N=333)),
231 in line with previous findings [5,8]. Early in infection (within 30 days of positive RT-PCR) neutralization
232 titers were significantly higher ($p<0.001$) and correlated better with binding parameters. As expected,
233 IgG responses to spike antigens showed the highest correlation with neutralization activity (Fig. 3b,
234 Supplementary Fig. 8-9). We next grouped patients based on the population into high (NT50 >250,
235 N=135) and no or low neutralizers (NT50 <250, N=332)[38] (Fig. 4a) and compared the prediction ability
236 of six different classification models to assign individuals based on their ABCORA 2.0 binding patterns
237 to these groups. Univariable logistic regression (ULR) models included only one variable: either the
238 mean of MFI-FOE S1 reactivities (ULR-S1), or the mean of MFI-FOE RBD reactivities (ULR-RBD). A
239 multivariable logistic regression (MLR) included both S1 and RBD mean reactivities. The additional

240 models included all 12 antigen reactivities measured in ABCORA and comprised a random forest
241 approach and two MLR strategies based on principle component analysis (PCA, 2 and 4 first axis).
242 Models were compared based on AUC and the BIC (Bayesian information criterion[39]) by cross
243 validation (Fig. 4b, c). All models performed similarly, with the univariable model based on the mean
244 of S1 reactivities (ULR-S1) yielding the best BIC value. Receiver operating curve (ROC) analysis based
245 on ULR-S1 showed a good capacity in predicting neutralization status yielding AUC 0.90 (N= 467, Fig.
246 4d). Exploring different cutoffs to balance sensitivity and specificity keeping both above 80%, we chose
247 to assign samples to the high neutralizers group if its predicted probability was above 70%. This
248 corresponds to an 83% specificity in correctly assigning non–neutralizers and 80% sensitivity in
249 assigning neutralizers (Fig. 4d, e). To increase the utility of the ULR-S1 prediction model for clinical
250 diagnostics, we devised a modified neutralization prediction model ULR-S1-SOC based on the SOC
251 values reported for ABCORA 2.0. At 70% predicted probability, ULR-S1-SOC delivers neutralization
252 prediction at similar sensitivity (81%) and specificity (81%) by examining if the composite S1 SOC value
253 (sum of S1 SOC values for IgG, IgA and IgM) is below or above 9.7 (Fig. 4f). Thus, based on ULR-S1-SOC
254 neutralization activity can be ranked directly from the basic SOC readout. We therefore conclude that
255 the basic readout in ABCORA 2.0 can deliver a reliable prediction of high neutralization activity.
256

257 **Resolution of temporal antibody dynamics by ABCORA seroprofiling**

258 Cross-sectional analysis of antibody reactivity post SARS-CoV-2 diagnosis by RT-PCR (N=369) and post
259 onset of symptoms (N=333) underlined the capacity of ABCORA seroprofiling to dissect onset, peak
260 and waning of SARS-CoV-2 antibody responses (Fig. 5a, b, Supplementary Fig. 10). In individuals with
261 known date of first SARS-CoV-2 RT-PCR diagnosis or onset of symptoms, ABCORA 2.3 detected early
262 seroconversion in 98% (48 of 49) and 100% (9 of 9) of individuals within 7 days post RT-PCR and onset
263 of symptoms, respectively. Besides IgM and IgA reactivity, IgG responses were readily detectable in
264 ABCORA 2.0 after a few days of infection (Supplementary Fig. 10).

265 Longitudinal assessment of a cohort of convalescent patients up to 11 months post infection (251
266 measurements on 120 patients) highlighted the temporal dynamics of SARS-CoV-2 binding antibodies.
267 We estimated the decay of binding reactivity employing a linear mixed model and identified a
268 significant reduction in RBD, S1, and N in all Ig subtypes (Fig. 5b) with half-lives ranging from 116 to
269 836 days, with IgG N titers decaying the fastest, in line with previous reports [10]. Half-lives of the
270 neutralization relevant IgG responses to RBD and S1 where 209 and 323 days, respectively. Intriguingly,
271 the kinetics of neutralizing antibodies did not mirror the decay rates observed for binding antibodies.
272 Neutralization activity decreased overall at a slower rate, with a half-life of 410 days (Fig 5c). This was
273 in part due to a mixed reactivity pattern with some individuals showing an increase in neutralization
274 activity post positive SARS-CoV-2 RT-PCR [5], while neutralization activity in others rapidly decayed
275 (Supplementary Fig. 10c).
276

277 **Interdependencies of SARS-CoV-2 and HCoV immunity**

278 To enable a more detailed analysis of HCoV antibody reactivity alongside SARS-CoV-2, we expanded
279 the bead antigen array to include S1 proteins of all four circulating HCoVs (HCoV-NL63, HCoV-229E,
280 HCoV-HKU1, HCoV-OC43) (Supplementary Fig. 11a). According to its capacity to monitor antibodies to
281 five coronaviruses we termed the assay ABCORA 5.0 and trained and validated it on the same cohorts
282 as ABCORA 2.0 (Fig. 1). To allow direct comparison with ABCORA 2.0 and use of the neutralization
283 prediction models, we used the threshold-/SOC-based analysis settings of ABCORA 2.0 also for ABCORA
284 5.0. Based on ABCORA 5.0 measurements of training cohorts I-III, we devised two random forest-based
285 analysis models. ABCORA 5.4 included solely the 12 SARS-CoV-2 parameters, ABCORA 5.5 included in
286 addition the S1 HCoV measurements adding up to 24 parameters in total. In analogy to ABCORA 2.3,
287 incorporation of HCoV reactivity into the model was advantageous. ABCORA 5.5 provided the highest
288 sensitivity and specificity amongst the analysis algorithms probed ABCORA 5.0 (Supplementary Fig.
289 11b, Supplementary Table 10).

290 Interdependencies between antibody reactivity to the four HCoVs and SARS-CoV-2 mirrored what we
291 previously observed for HKU1 with a particular high correlation of IgM reactivity of SARS-CoV-2 and
292 HCoVs in pre-pandemic individuals, particularly in those with recent HCoV infection (Supplementary
293 Fig. 12). HCoV infections are frequent but subject to seasonality and prevalence of individual HCoV
294 infections fluctuates [40,41]. In line with this, the prevalence of HCoV responses measured by ABCORA 5.0
295 in local blood donors in January 2019 (N=285), May 2019 (N=288), and January 2020 (N=252) varied
296 considerably (Fig. 6). To enable a time-controlled comparison of HCoV reactivity between SARS-CoV-
297 2-infected and healthy donors, we screened blood donors from May 2020 (N=672), when SARS-CoV-2
298 prevalence was estimated below 2% in Zurich, Switzerland [42], by ABCORA 2.0/5.0 and excluded all
299 samples with SARS-CoV-2 reactivity. The residual May 2020 cohort (N= 653) formed a pandemic,
300 healthy donor control group. Interestingly, HCoV reactivity patterns in 2019 and 2020 differed
301 substantially as assessed by one-way ANOVA, with January 2020 showing the comparatively lowest
302 and May 2020 the highest IgA and IgG reactivity, which may indicate a later onset of an HCoV epidemic
303 in 2020 compared to 2019 (t-tests of May 2020 versus other groups shown in Fig. 6).
304 Most intriguingly, a time-matched analysis comparing May 2020 healthy donors with SARS-CoV-2-
305 positive patients sampled in April, May and June 2020 (N=65) revealed significantly lower HCoV
306 reactivity in SARS-CoV-2 positive patients (Fig. 7a). This pattern was also evident when we extended
307 the analysis to include the full cohort of SARS-CoV-2 infected individuals measured with ABCORA 5.0
308 (N=389, sampled from March 2020 to February 2021, Supplementary Fig. 13). Overall, this raised the
309 possibility that pre-existing immune responses to HCoVs may to a certain degree protect against SARS-
310 CoV-2 infection. We therefore investigated whether HCoV responses are linked to the evolution of
311 SARS-CoV-2 antibodies in patients with known date of first positive RT-PCR (SARS-CoV-2 patients
312 measured in ABCORA 5.0 with time since positive RT-PCR<60 days, N=204). Associations were
313 investigated with a linear regression model adjusted for age, gender, time since positive RT-PCR and
314 HCoV reactivity. To stratify HCoV reactivity into high and low HCoV activity, median logMFI-FOE were
315 defined for each HCoV and antibody class. LogMFI-FOE higher than the corresponding median for at

316 least three HCoVs (HKU1, OC43, NL63 or 229E) in a specific Ig class were ranked as having high HCoV
317 activity within this class. First, only reactivities among the same antibody class were explored in the
318 model (i.e. HCoV IgG high on SARS-CoV-2 IgGs). We observed exceptionally strong interdependencies
319 for IgA and IgM responses to SARS-CoV-2, which all were significantly higher in individuals with high
320 HCoV reactivity (Fig. 7b). This strongly suggests that pre-existing HCoV immunity may provide an
321 advantage in mounting SARS-CoV-2 responses. Interdependencies between HCoV IgG and SARS-CoV-
322 2 specific IgG were only observed for the S2 response. To explore if SARS-CoV-2 IgG may build on recent
323 HCoV IgA and IgM responses we next probed whether HCoV IgM and IgA are linked to elevated SARS-
324 CoV-2 specific IgG levels. While no effect was evident for IgM, we observed a significant association of
325 high HCoV IgA activity on all four measured SARS-CoV-2 responses (Fig. 7c, d). This strongly suggests
326 that recent HCoV infection has a beneficial effect on mounting SARS-CoV-2 antibody responses.
327

328 **Discussion**

329 Definition of SARS-CoV-2 immunity post vaccination and infection is of immediate importance [43-45].
330 Deciphering antibody correlates of SARS-CoV-2 protection and monitoring vaccine responsiveness are
331 challenging tasks ahead. The magnitude and longevity of protective antibody responses to natural
332 infection and of different vaccines need to be examined to understand parameters that shape
333 protective responses and guide decisions on re-vaccination in non-responders and immunization
334 against novel arising SARS-CoV-2 variants [46]. Likewise, creating means to serologically distinguish
335 between de novo infection, re-infection, and vaccine responses, their durability and failures will be
336 critical for clinical diagnosis.

337 Here we demonstrate the high utility of multi-parameter seroprofiling in addressing key issues in
338 defining SARS-CoV-2 immunity. We designed SARS-CoV-2 seroprofiling tests, termed ABCORA, to
339 address research and clinical diagnostics needs. Simultaneous recording of antibody responses to a
340 range of SARS-CoV-2 antigens and different Ig classes with ABCORA seroprofiling yields an extensive

341 picture on the SARS-CoV-2 serology status in a single assessment. High accuracy in defining SARS-CoV-
342 2 seropositivity and staging of seroconversion was achieved by a computational analysis. Validation
343 and verification of the performance of ABCORA against internal and external standards proved its
344 exceptional performance enabling application in clinical diagnostics and research.

345 Measuring neutralization will remain the ultimate goal to determine protective immunity to infection
346 and immunization. Protective activity against novel arising SARS-CoV-2 variants needs to be
347 determined [46-51]. Collecting information on neutralizing activity in large population groups is however
348 challenging as cell-based neutralization assays are not in wide diagnostic use and have limited turnover
349 and scalability. Means to derive estimates of neutralization activity based on comparatively simpler
350 binding assays would therefore provide an enormous advantage as previously suggested [52-54]. As we
351 demonstrate, computational modeling allows predicting plasma neutralization capacity from ABCORA
352 seroprofiling results, obliterating the need to conduct labor-intensive and costly neutralization tests in
353 clinical diagnostics or in large-scale research-based screens. The same principle can be applied in future
354 assay extensions to predict neutralization activity against novel SARS-CoV-2 variants.

355 The successful development of a sensitive seroprofiling test enabled a precise analysis of SARS-CoV-2
356 antibody dynamics and their interplay with HCoV responses. We utilized two ABCORA assay versions
357 that both measured HCoV reactivity alongside the 12 SARS-CoV-2 parameters. ABCORA 2 included the
358 S1 antigen of HKU1. ABCORA 5 included S1 of all four circulating HCoVs. Notably, computational
359 models that included the HCoV measurements allowed a higher precision in determining SARS-CoV-2
360 seropositivity, highlighting interdependencies between HCoV and SARS-CoV-2 responses that need to
361 be resolved. Recording reactivity against all four HCoVs in SARS-CoV-2 uninfected and infected
362 individuals we observed intriguing associations. Uninfected individuals displayed higher HCoV
363 reactivity compared to infected individuals. However, amongst persons with documented SARS-CoV-2
364 infection, those with high HCoV reactivity developed higher SARS-CoV-2 antibody levels. While
365 association studies as ours cannot formally define causality, the implications of our findings are
366 evident: Prior immunity to HCoV may protect to some extent against SARS-CoV-2 acquisition and may

367 provide a boost to the development of SARS-CoV-2 specific immunity. While we solely measured
368 antibody responses, a potential protective effect of HCoV immunity against SARS-CoV-2 acquisition
369 should not be viewed restricted to antibody activity. Antibodies and cellular immunity may both be
370 relevant and act in concert [55-57]. Alternatively, antibody responses measured in the present study may
371 solely document recent HCoV infection and deliver a surrogate measurement of other protective HCoV
372 responses. The link between higher HCoV and SARS-CoV-2 reactivity in infected individuals is
373 particularly intriguing. Strongest effects were seen for IgM and IgA HCoV responses, suggesting that
374 recent HCoV immunity provides an early boost to SARS-CoV-2 antibody development. Whether this is
375 due to cross-reactive B cell responses on which the SARS-CoV-2 immunity builds on and matures or
376 whether cross-reactive T helper activities play a role will be important to resolve in forth-coming
377 studies. Likewise the precise role and timing of the HCoV responses that shape SARS-CoV-2 antibody
378 responses needs to be defined. Early, low affinity HCoV responses may have a positive impact for the
379 evolution of SARS-CoV-2 immunity by providing an immune memory to build on, while the boosting of
380 non-protective cross-reactive HCoV antibodies may have a negative impact following the antigenic sin
381 principle [30].

382

383 Our findings have multiple implications and warrant further investigation of the interplay between
384 HCoV and SARS-CoV-2 immunity. A modest protective effect by HCoV immunity would be a plausible
385 explanation for the high proportion of asymptomatic and mild SARS-CoV-2 infections [58,59]. Even more
386 intriguing are future perspectives. As others and we have shown, SARS-CoV-2 and HCoV immunity to
387 infection is often not long-lasting (Fig. 5, Supplementary Fig. 10) [5,60], a limitation that SARS-CoV-2
388 vaccines hope to overcome. Should SARS-CoV-2 responses in turn provide a degree of defense against
389 HCoV infection, broad protection against coronaviruses may be in reach.

390

391 **Methods**

392 **Human specimen**

393 Serum and plasma samples collected pre and post emergence of SARS-CoV-2 in Switzerland (pre and
394 post February 2020, respectively) were included. No patient enrollment was conducted for the present
395 study. All experiments involving samples from human donors were conducted with the approval of the
396 responsible local ethics committee Zurich, Switzerland (BASEC Nrs 2020-01327, 2020-00363; Req-
397 2021-00437; 2020-00787), in accordance with the provisions of the Declaration of Helsinki and the
398 Good Clinical Practice guidelines of the International Conference on Harmonisation. Samples were
399 obtained from the following sources: i) Zurich blood donation services (ZHBDS): Anonymized healthy
400 adult plasma from pre-pandemic time points (January 2019, May 2019 and January 2020) and from
401 the first wave of the pandemic in Zurich, Switzerland (May 2020) were provided by the ZHBDS internal
402 serum repository (BASEC 2020-00363). ii) Anonymized leftover specimens from routine diagnostics at
403 the Institute of Medical Virology, University of Zurich, the University Children Hospital Zurich and the
404 Cantonal Hospital Winterthur (BASEC Nrs 2020-01327, Req-2021-00437). iii) Healthcare workers with
405 RT-PCR confirmed SARS-CoV-2 infection participating in a study at the University Hospital Zurich
406 (BASEC 2020-00363). iv) Male plasma donors participating in a SARS-CoV-2 plasma therapy study
407 conducted at the University Hospital Zurich (CPT-ZHP, Swissmedic 2020TpP1004; BASEC 2020-00787).
408 Pre-pandemic (SARS-CoV-2 negative, N=825) and confirmed SARS-CoV-2 positive samples (N=389)
409 were divided into training and validation cohorts (Supplementary Table 3). The SARS-CoV-2 training
410 cohort (N=175) included plasma collected during infection (N=114) and convalescence (N=61). Per
411 donor only one sampling time point was included, longitudinal samples of donors included in the
412 training cohort were not included in the validation cohort to ascertain independence when assessing
413 the sensitivity and specificity of the different diagnostic methods. The SARS-CoV-2 validation cohort
414 (N=214), comprised plasma collected during infection (N=90, one sampling time point per donor) and
415 convalescence (N=124, 79 convalescent patients with 1-4 longitudinal samples). Multiple time points
416 of convalescent patients were included in the validation data set to capture a wide spectrum of waning

417 antibody titers. Cross-sectional analysis was based on samples with known time since positive RT-PCR
418 (N=369) or known time since symptom onset (N=333), both including the longitudinal analysis
419 observations. Both, time since positive RT-PCR and time since onset were known for 330 samples, with
420 a median time of 3 days between symptom onset and RT-PCR (1st-3rd quartile: 1-7 days). Longitudinal
421 analysis of antibody reactivity was based on 251 observations from 120 convalescent patient with
422 known time since positive RT-PCR and time since symptom onset. Neutralization was measured on 467
423 SARS-CoV-2 RT-PCR positive samples (N=369 with known time since positive RT-PCR, N=333 with
424 known time since symptom onset).

425 We further evaluated cross-reactivity ABCORA 2.0 and 5.0 in left-over plasma from routine diagnostics
426 in a pre-pandemic control group with documented, recent HCoV infection (Training II, N= 75, OC43
427 (N=27), HKU1 (N=17), NL63 (N=22), 229E (N=9)). Circulating HCoV are commonly only screened for in
428 in hospitalized, severe respiratory infections and immune compromised individuals who routinely
429 undergo a broad screening for respiratory infections. Hence, in this patient group both, reduced
430 antibody reactivity due to immune compromising or elevated HCoV antibody reactivity due to recent
431 or recurring HCoV infection may occur. As this group is diagnostically relevant we considered it prudent
432 to include this cohort as Training II data set to verify if cross-reactivity with SARS-CoV-2 in ABCORA
433 occurs in this setting. Training II data were not included in the threshold definition to not over-
434 represent individuals with severe illness. This HCoV infected group displayed overall lower reactivity
435 with SARS-CoV-2 than plasma from healthy adults but importantly showed no indication of cross-
436 reactivity (Fig. 1a, b). Pandemic samples from anonymous blood donors with unknown SARS-CoV-2
437 status collected in May 2020 (N=672) were not included in training and validation cohorts.

438

439 **Reagents and cell lines**

440 His-tagged SARS-CoV-2-derived antigens (receptor binding domain (RBD), subunit S1 (S1), subunit S2
441 (S2), nucleocapsid protein (N)) and S1 of the four circulating HCoVs (HKU1, OC43, NL63, 229E) were

442 purchased from Sino Biological Europe GmbH, Eschborn, Germany (Supplementary Table 12). Sources,
443 specifics and concentration of detection and control antibodies and sera used for ABCORA and
444 neutralization tests are listed in Supplementary Table 13. 293-T cells were obtained from the American
445 Type Culture Collection (ATCC CRL-11268) [61]. HT1080/ACE2cl.14 cells [32] were kindly provided by P.
446 Bieniasz, Rockefeller University, NY. Both cell lines were cultured in DMEM containing 10% FCS.

447

448 **Design of multiplex bead assay ABCORA 2.0**

449 We established two bead-based multiplexed SARS-CoV-2 immunoassays (ABCORA 2.0 and ABCORA
450 5.0) that included a range of SARS-CoV-2 and HCoV antigens (Sino Biological Europe GmbH, Eschborn,
451 Germany, Supplementary Table 12). Four SARS-CoV-2 antigens - RBD, S1, S2 and N - were included in
452 both ABCORA 2.0 and ABCORA 5.0. ABCORA 2.0 included in addition S1 of HCoV-HKU1, ABCORA 5.0
453 included S1 of all circulating HCoVs (HCoV-NL63, HCoV-229E, HCoV-HKU1, HCoV-OC43). In brief,
454 individual MagPlex beads (Luminex Corporation, Austin, TX) with unique fluorescent bead regions were
455 chosen for each antigen, beads were coupled and mixtures of antigen-coupled beads incubated with
456 patient plasma in a 96-well plate set-up. Median Fluorescent Intensity (MFI) of bead-bound plasma
457 antibodies were measured utilizing a FlexMap 3D reader (Luminex Corporation, Austin, TX). We
458 designed the assay to fulfil the following criteria: i) high specificity, sensitivity and reproducibility, ii)
459 flexible multiplex design that allows straightforward addition and/or alteration of antigens; iii) wide
460 dynamic range; iv) optional quantification of antibody responses; v) optional recording of antibody
461 responses to HCoVs and vi) use in routine diagnostics and research.

462 We chose a sterically orientation capture via anti-His antibodies to ensure a homogenous antigen
463 display. Therefore, carboxylated MagPlex beads (Luminex Corporation, Austin, TX) were coupled with
464 anti-His antibody (Sino Biological Europe GmbH, Eschborn, Germany, Supplementary Table 10) and
465 then coupled with His-tagged antigens using Bio-Plex Amine coupling (Bio-Rad Laboratories AG,
466 Cressier, Switzerland) according to the manufacturer's instructions and as described [62].

467 Serum/plasma titration is in general considered the most accurate strategy to retrieve quantitative
468 information on antibody reactivity. However, in diagnostic use tests ideally should deliver (semi)-
469 quantitative information from a single serum dilution to permit a sufficient throughput. The finalized
470 assay conditions covered a 2-log MFI range across all probed antigen-Ig combinations (Supplementary
471 Fig. 2). Ratifying the validity of using a single plasma dilution, we confirmed that plasma from SARS-
472 CoV-2 positive patients and pre-pandemic SARS-CoV-2 negative plasma samples show optimal dose
473 response curves over a wide plasma dilution range (Supplementary Fig. 2d). Importantly, a 1/100
474 dilution of plasma was in all cases close to the maximum signal, underlining that increasing plasma
475 concentration would not increase signal intensity but rather endanger decreasing signals due to
476 prozone effects (Supplementary Fig. 2d).
477 Maximal anti-His antibody loading was achieved at 5 µg antibody per million beads (Supplementary
478 Fig. 2) and used as standard coupling condition. In the final protocol, five million anti-His antibody
479 coupled magnetic beads were incubated with His-tagged antigens diluted in PBS at a concentration of
480 320 nM. Phycoerythrin (PE)-labeled secondary antibodies specific to IgG, IgA or IgM were used as
481 detector antibodies (Supplementary Table 13). Quality control of the antigen loading was performed
482 by incubating the beads with monoclonal antibodies targeting the corresponding CoV-derived antigen
483 as detailed in Supplementary Table 12. Analysis was performed with the FlexMap 3D reader (Luminex
484 Corporation, Austin, TX) with the acquisition of at least of 50 beads per bead region. Results are
485 recorded as MFI per bead region.

486 Several control measures were installed to ascertain inter- and intra-assay performance. To ascertain
487 a low assay-to-assay variability, large batches of individual antigen-loaded beads were prepared and
488 frozen in aliquots until use at -20°C to circumvent decay of the antigen-coupled beads (Supplementary
489 Fig. 1). Individual coupled beads were mixed on the test day to yield the required antigen bead cocktail.
490 Cocktails contained 60 beads per bead region per µl. In addition to the SARS-CoV-2 and HCoV bead
491 regions, each cocktail included an empty bead region (no antigen coupled) to control for unspecific
492 binding. Quality control and validation procedures for the FlexMap 3D instrument were done on each

493 day of experiment according to manufacturer's instructions. The variability of the assay was analyzed
494 as described previously [62]. In brief, plasma samples from 20 RT-PCR confirmed SARS-CoV-2 infected
495 patients were pooled and tested over a range of seven dilutions in 31 different titrations performed
496 on 10 different days (Supplementary Fig. 3). Across all antigens and Ig classes, signals were retained
497 over the test period of 25 days post bead coupling. Coefficients of variation (CV) of the binding signal
498 across titrations of the 12 antigen-Ig class combinations proved low (range: 0.010-0.128, median 0.059,
499 Supplementary Fig. 4c, d, Supplementary Tables 1, 2). Same-day and day-to day variability proved low
500 and comparable (Supplementary Fig. 4e, f). Below a 1/100 plasma concentration, CV increased
501 markedly (Supplementary Fig. 4d), defining 1/100 as highest concentration (lowest plasma dilution) to
502 be tested in the assay. A 1/100 plasma dilution was thus defined as the basic dilution for screening
503 plasma in ABCORA 2.0 when a qualitative (i.e. presence or absence of SARS-CoV-2 specific antibodies)
504 or semi-quantitative (i.e. MFI signal intensity) readout is required.

505 All ABCORA measurements were derived from single measurements unless stated otherwise. To
506 measure SARS-CoV-2 specific antibodies in patient plasma, heat inactivated plasma (1 h at 56°C) was
507 diluted 1/100 in PBS-BSA 1% unless otherwise stated. 50 µl diluted plasma were incubated with 50 µl
508 of the ABCORA antigen bead cocktail for 30 minutes at room temperature in 96-well plates, washed
509 three times with PBS-BSA 1% and incubated in separate reactions with phycoerythrin (PE)-labeled
510 detector antibodies for IgG, IgA or IgM at a final concentration of 1/500 in PBS-BSA 1%. This dilution
511 was previously defined by titration of the detector antibodies to yield optimal MFI signals. After 45
512 minutes of incubation at room temperature, beads were washed three times with PBS-BSA 1% and
513 analyzed in 96-well plates on the FlexMap 3D reader (Luminex Corporation, Austin, TX). A minimum of
514 50 bead reads per antigen was acquired.

515 To control for genuine cross-reactive antibodies, each plasma sample was assessed with beads without
516 antigen (empty bead control) in combination which each detector antibody. For analysis, raw MFI
517 values were transformed to MFI-FOE to correct for background binding. We established mean empty
518 bead MFI-FOE for IgG, IgA and IgM of pre-pandemic healthy donors (N=1016) and set the mean MFI-

519 FOE + 4x standard deviation as threshold for the empty bead control. In absolute levels, these
520 thresholds amounted to MFI-FOE 41.58 (IgG), 55.91 (IgA) and 269.47 (IgM). Measurements for which
521 the empty bead control recorded values above this threshold were considered invalid and repeated.
522 Each Luminex analysis 96-well plate was set up to contain the same set of control samples
523 (Supplementary Fig. 1c), namely 7 serial 4-fold dilutions of a SARS-CoV-2 positive control donor pool
524 (N=20 donors, starting dilution 1/100, Supplementary Fig. 2d) and a pre-pandemic healthy donor pool
525 (dilution 1/100, N=20 donors, Supplementary Fig. 2d). These positive and negative controls allow to
526 control assay performance across independent measurements and in addition enable retrospective
527 standardization against external controls if needed.
528

529 **Definition of SARS-CoV-2 seropositivity in ABCORA 2.0 and ABCORA 5.0**

530 Individual MFI-FOE cut-off values for SARS-CoV-2 specific responses for each of the 12
531 antigen/immunoglobulin combinations were set for ABCORA 2.0 based on the training cohorts
532 (Supplementary Table 4). Threshold levels were set to reach an overall specificity above 99% and
533 included levels for border-line reactivity for IgG RBD, IgG S1 and IgG N to allow also modest antibody
534 reactivity to these antigens to be examined. MFI-FOE reads of individual samples were transformed
535 into signal-over cut-off (SOC) values (MFI-FOE/threshold). SOC values are used for assessing positive
536 reactivity for each individual antigen-antibody class combination, with SOC>1 denoting positive
537 reactivity, SOC<1 denoting negative reactivity. When setting individual thresholds, it must be
538 considered that for each of the 12 probed activities cross-reactivities may occur. With 12 individual
539 SOC parameters recorded, overall specificity will decrease if any positive SOC independently suffices
540 to rate a sample overall as SARS-CoV-2 antibody positive. To exemplify: Assuming independent
541 responses, even a high 99% specificity for each antigen will add up to an overall low 88% specificity
542 across the entire assay. We thus required for SARS-CoV-2 positive calling in ABCORA 2.0 a minimum of
543 two specificities to reach activity above threshold. The combined SOC values used to define the overall
544 serostatus of a given sample are detailed in Supplementary Table 5. For IgG RBD, S1 and N, for which

545 we also recorded border-line SOC activity, we allowed for a combination of 1 antigen reactivity SOC>1,
546 the second reactivity SOC> border line. The final threshold and positive call criteria allowed for a
547 differentiation of partial (partial (early seroconversion with only IgM and IgA responses) to full
548 seroconversion (including IgG responses) (Supplementary Table 5). In addition, the criteria denote
549 samples with weak reactivity and/or indeterminate reactivity (Supplementary Table 5).

550 To ease comparison between ABCORA 2.0 and ABCORA 5.0 the same threshold cut-offs were used for
551 ABCORA 5.0. We chose not to create specific cut-off thresholds for HCoV antibody reactivity as an
552 accurate definition of a negative response is complex due to the wide-spread exposure to HCoVs and
553 considerable antibody cross-reactivity between them. HCoV responses were however included in the
554 statistical analyses as MFI-FOE values.

555

556 **Definition of SARS-CoV-2 seropositivity using logistic regression classification**

557 Classification of seropositive versus seronegative samples in ABCORA 2.1 was realized using logistic
558 regression. The identical training and validation data used for the establishment for ABCORA 2.0 were
559 used. As the ABCORA 2.0 binding reactivities were highly correlated, we included the following
560 variables in the model (Supplementary Fig. 6a): the mean value of all IgG MFI-FOE responses (RBD, S1,
561 S2, N), the mean value of the IgA MFI-FOE responses against RBD, S1 and S2, and the mean value of
562 the IgM MFI FOE responses against RBD, S1 and S2. IgA and IgM responses to N were excluded as they
563 were not clustering with the other responses of the same Ig class (Supplementary Fig. 6a). The logistic
564 regression was used to estimate and predict the probability of a given sample to be positive (p) as
565 follows:

566 $$p = \frac{\exp(\beta 0+\beta G*mean(IgG{:}RBD,S1,S2,N)+\beta A*mean(IgA{:}RBD,S1,S2)+\beta M*mean(IgM{:}RBD,S1,S2))}{1+\exp(\beta 0+\beta G*mean(IgG{:}RBD,S1,S2,N)+\beta A*mean(IgA{:}RBD,S1,S2)+\beta M*mean(IgM{:}RBD,S1,S2))}$$

567 Parameters $\beta 0$, βG, βA and βM were estimed on the training dataset. A sample was then defined as
568 positive if its predicted probability of being positive was above a threshold c'. This threshold was

defined as to obtain a specificity of at least 0.99 and maximal sensitivity on the training dataset (similarly to c for the random forest). In summary, in ABCORA 2.1, any new sample is defined as seropositive if its probability of being seropositive as estimated by the logistic regression is above c'. Analyses were performed in R version 3.6.3.

Definition of SARS-CoV-2 seropositivity using random forest classification

Classification of seropositive versus seronegative samples in context of ABCORA 2.0 and ABCORA 5.0 was realized using a random forest approach following the basic setup of random forests as described in[63]. The random forest itself was built of an ensemble of 1000 classification trees using MFI-FOE responses (IgA, IgG and IgM against RBD, S1, S2, N). The probability of a sample being positive as predicted by the random forest is the average of the probabilities over all 1000 trees. Finally, a sample is defined as positive if its probability of being positive is above a threshold c, which is defined as to obtain a specificity of at least 0.99 and a maximal sensitivity on the training dataset. In summary, any new sample is defined as seropositive if its probability of being seropositive as estimated by the random forest is above the threshold c. We conducted a series of random forest analyses that considered either only SARS-CoV-2 responses or SARS-CoV-2 and HCoV responses in ABCORA 2.0 and ABCORA 5.0: ABCORA 2.2 and ABCORA 2.3 were trained and used for prediction on ABCORA 2.0 data and included only SARS-CoV-2 responses or SARS-CoV-2 and HKU1 responses, respectively. ABCORA 5.4 (SARS-CoV-2 responses only) and ABCORA 5.5 (SARS-CoV-2 and HCoV responses) were trained on ABCORA 5.0 data. Details on the data inclusion for the respective models are listed in Supplementary Table 3 and Supplementary Table 10. Analyses were performed in R version 3.6.3 using packages random Forest and ranger [64-67].

594 **Validation and verification using external controls**

595 We used the Anti-SARS-CoV-2 Verification Panel for Serology Assays (NIBSC code: 20/B770, NIBSC) to
596 verify the performance of the ABCORA 2.0 and ABCORA 2.3 test. Serum samples of the verification
597 panel measured by ABCORA 2.0/2.3 as described and results compared with the results of
598 commercially available assays reported by the NIBSC ([31] and Supplementary Table 6). We further
599 verified the sensitivity of the ABCORA 2 test in detecting SARS-CoV-2 infection in a direct comparison
600 with commercial tests. Antibody status of plasma from SARS-CoV-2 positive individuals (N=171) were
601 analyzed with the following test systems: Included test systems targeted the N protein (Elecsys® Anti-
602 SARS-CoV-2 (Roche Diagnostics GmbH)), the RBD region of the S protein (Elecsys® Anti-SARS-CoV-2 S
603 assay (Roche Diagnostics GmbH)), and the S1 subunit (EUROIMMUN Anti-SARS-CoV-2 ELISA (IgG))
604 (Supplementary Table 7). All assays were performed according to the manufacturer's instructions in
605 the diagnostics unit of the Institute of Medical Virology, University of Zurich, Switzerland.

606

607 **SARS-CoV-2 binding antibody titers**

608 To define binding antibody titers, 8 serial 4-fold dilutions starting with a 1/25 dilution of plasma were
609 prepared and measured in ABCORA 2.0. To derive quantitative information, MFI values were corrected
610 for background activity (MFI-empty bead control) and we defined the area under the MFI curve (AUC)
611 across the dilution series for each antigen-Ig combination. As a second quantitative readout, we
612 calculated 50% effective titer concentrations (EC50) using a four-parameter logistic curve
613 (y=Bottom+(Top-Bottom)/(1+10^((logEC50-X)*HillSlope).

614

615 **Quantification of SARS-CoV-2 S1 and RBD activity**

616 We used two approaches to standardize SARS-CoV-2 S1 and RBD activity. The first was based on the
617 S1/RBD specific antibody CR3022 ([37] and Supplementary Table 13). Serial dilutions of IgG, IgA and IgM

618 versions of CR3022 were used to create standard curves on RBD and S1 coated beads. The linear range
619 of the standard and sample dilution curve was used for quantitation. We fitted a four-parameter
620 logistic curve (y=Bottom+(Top-Bottom)/(1+10^((logEC50-X)*HillSlope) (Supplementary Fig. 7b)
621 through which MFI values of measured samples are interpolated into a corresponding concentration
622 of antibody (µg/ml). We used this approach to quantify the concentration of RBD and S1 antibody
623 reactivity in the positive donor control, and used titrations of the donor pool included on each ABCORA
624 plate to calculate the S1 and RBD content of plasma samples in relation to it. We used the same
625 strategy in combination with the WHO International Standard Anti-SARS-CoV-2 Immunoglobulin
626 (NIBSC 20/136 [31]) to defer IU/ml content of the internal ABCORA positive donor pool and the individual
627 specimen tested (Supplementary Fig. 7). The WHO International Standard consists of a pool of plasma
628 from individuals with confirmed SARS-CoV-2 infection. RBD and S1 content of the ABCORA positive
629 donor pool quantified via the polyclonal WHO standard was highly similar within each Ig class
630 (Supplementary Fig. 7b). In contrast, RBD values estimated by the mAb CR3022 were a factor 2.4 – 3.9
631 lower than the corresponding S1 values, suggesting an affinity difference of CR3022 for the two
632 antigens (Supplementary Fig. 7b).

633

634 **Temporal evolution of SARS-CoV-2 binding antibody response**

635 Antibody binding of 140 convalescent patients was measured longitudinally in 274 measurements with
636 ABCORA 2.0, including 251 measurements from 120 patients with known time since positive RT-PCR.
637 We assumed the dynamics of antibodies (analyzed as logMFI-FOE) were following a linear trend with
638 time and estimated the slope using a linear mixed model with random effect on the intercept. As time
639 measures days post first positive RT-PCR result (Fig. 5b) or days post onset of symptoms
640 (Supplementary Fig. 9b) were employed. Half-lives (t1/2, in days) of significant response with negative
641 slopes were calculated based on the respective estimated slopes. Analyses were performed in R
642 version 3.6.3 using packages lme4 [68] and lmerTest [69].

643 **SARS-CoV-2 pseudo-neutralization assay**

644 SARS-CoV-2 plasma neutralization activity was defined using an HIV-based pseudovirus system as
645 described [32]. The env-inactivated HIV-1 reporter construct pHIV-1NL4-3 ΔEnv-NanoLuc (pHIV-
646 1Nanoluc) and HT1080/ACE2cl.14 cells were kindly provided by P. Bieniasz, Rockefeller University, NY,
647 USA. To create a SARS-CoV-2 spike expression plasmid (P_CoV2_Wuhan), a codon-optimized C
648 terminal truncated (AA 1255-1273) spike encoding gene of strain Wuhan-Hu-1 (GenBank accession no.
649 MN908947) was synthesized (GeneArt, Thermo Fisher Scientific, Waltham, MA) and cloned into
650 pcDNA.3.1. Pseudotyped SARS-CoV-2 spike expressing viruses were generated by co-transfecting 293-
651 T cells with a mixture of pHIV-1Nanoluc, P_CoV2_Wuhan and PEI Max (Polysciences Europe GmbH,
652 Hirschberg, Germany). After 48h virus supernatants were filtered (0.2 µm) and stored in aliquots at -
653 80°C until use. Infectivity of virus stocks was measured by infection of HT1080/ACE2cl.14 cells. For this
654 384-well culture plate pre-treated with poly-L-Lysin were seeded with HT1080/ACE2cl.14 (2200
655 cells/well) one day before the assay. Cells were infected with titrated virus stocks and NanoLuc
656 luciferase activity in cell lysates measured 48 h post infection using the Nano-Glo Luciferase Assay
657 System (Promega, Fitchburg, WI). For this, cells were washed once with PBS, supernatant was removed
658 and cells were lysed with 20 µl/well of Luciferase Cell Lysis reagent (Promega, Fitchburg, WI) for 15
659 min under continuous shaking at room temperature. 20 µl of 1/ 50 diluted NanoGlo buffer were added
660 and NanoLuc luciferase activity (relative light units, RLU) was measured after 5 min incubation at room
661 temperature on a Perkin Elmer EnVision reader. Input of SARS-CoV-2 pseudoviruses for neutralization
662 assays was adjusted to yield virus infectivity corresponding to 5-10 x10^6 RLU (corresponding to 100-
663 250-fold over background RLU values) in the absence of inhibitors. To measure plasma neutralization
664 activity six serial 4-fold dilutions of plasma starting at a 1/25 dilution were prepared. 20 µl of the diluted
665 plasma and 20 µl of virus were pre-incubated for 1 h at 37°C and then 30 µl of the virus/plasma mix
666 were transferred to 384-well plates seeded with HT1080/ACE2cl.14 cells in a volume of 30 µl. This
667 resulted in a final concentration of the plasma starting dilution of 1/100. Plasma neutralization titers
668 causing 50%, 80% and 90% reduction in viral infectivity (NT50, NT80 and NT90, respectively) compared

669 to controls without plasma were calculated by fitting a sigmoid dose–response curve (variable slope)
670 to the RLU data, using GraphPad Prism with constraints (bottom=0, top=100). If 50% inhibition was not
671 achieved at the lowest plasma dilution of 1/100, a 'less than' value was recorded. All measurements
672 were conducted in duplicates.

673

674 **Predicting neutralization based on ABCORA binding activity**

675 To compare the ability of SARS-CoV-2 binding activity measured in ABCORA 2.0 to predict the
676 neutralization status, we measured neutralization activity to Wuhan-Hu-1 in SARS-CoV-2 positive
677 individuals (N=467) and classified individuals as high neutralizers (NT50 >250, N=332) and low
678 neutralizers (NT50 <250, N=135). Six different classification models were designed to assign individuals
679 to the high or low neutralizers category, based on their ABCORA2.0 binding patterns we established
680 two univariable logistic regression (ULR) models that included mean MFI-FOE spike antigen S1
681 reactivities and mean MFI-FOE spike antigen RBD reactivities, respectively. S1 and RBD were chosen
682 due to their highest correlation with NT50 (r= 0.82 and r=0.80 for the total spike reactivities of S1 and
683 RBD respectively, Supplementary Fig. 9). In addition to these two ULR, we established a multivariate
684 logistic regression model including both mean S1 and RBD reactivities (MFI). We further devised three
685 models that considered all 12 SARS-CoV-2 binding parameters recorded by ABCORA 2.0. Two
686 multivariable logistic regression models were based on a principal component analysis on all binding
687 activities and included the first two (respectively four) principal components, which explained 60%
688 (respectively 75%) of the variance in the data. We also included in our model comparison a
689 classification based on a random forest analysis that incorporated all 12 SARS-CoV-2 binding activity
690 variables.

691 For all 6 models, performance was assessed in 100 cross-validation sets: each set was built by randomly
692 sampling without replacement among the 467 measurements available. 80% of the data set was used
693 to train the model (N=374). Prediction of neutralization status was realized on the other 20% (N=93)

694 and compared to the true NT50 value and neutralization status, using a roc curve. The area under the
695 curve (AUC) was computed for all 6 models in each cross-validation run. The Bayesian information
696 criterion (BIC) was computed for all 5 logistic regressions in each cross-validation run.

697 To increase the utility of the ULR-S1 prediction model for clinical diagnostics we devised a modified
698 neutralization prediction model ULR-S1-SOC based on the signal over cut-off (SOC) values reported for
699 ABCORA 2.0. The ULR-S1-SOC estimates the probability of NT50>250 based on the sum of S1 SOC
700 values for IgG, IgA and IgM as follows:

701

702 $$P(NT50 > 250) = \frac{\exp(a + b * log10(sum\ S1\ SOC))}{1 + \exp(a + b * log10(sum\ S1\ SOC))}$$

703

704 With estimated values: a= -2.6447 and b= 3.5353.

705

706 **Association between HCoVs and SARS-CoV-2 reactivities**

707 To explore the association between HCoVs and SARS-CoV-2 reactivities, we defined a new HCoV
708 response variable (HCoV high/low) for each antibody class (IgG, IgA, IgM) as follows: a patient had high
709 HCoV Ig reactivity for a given antibody class if its measurements were higher than the population
710 median in at least three out of the four HCoV measurements (HKU1, OC43, NL63, 229E). To assess
711 interdependencies between HCoV and SARS-CoV-2 responses, we then included the HCoV response
712 variable in a linear regression model of SARS-CoV-2 reactivities in the same antibody class. The linear
713 regression models were estimated on a subset of SARS-CoV-2 positive patients (N=204), measured on
714 ABCORA 5.0 less than 60 days since positive RT-PCR. The restriction to 60 days was chosen to allow
715 modeling the effect of time with splines. This time period restriction further guaranteed a gender
716 balance, as convalescent donors with longer follow up were all males recruited for a plasma therapy
717 study (CPT-ZHP, Swissmedic 2020TpP1004). Regression analyses were adjusted on time (days post

718 positive RT-PCR or onset of symptoms; as a spline with 3 degrees of freedom), age (as a spline with 3
719 degrees of freedom) and gender.
720
721 **Statistical analysis**
722 Statistical analyses were performed in R (Version 3.6.3). Figures were made using the ggplot2
723 package[70]. When included, boxplots represent the following: median with the middle line, upper and
724 lower quartiles with the box limits, 1.5x interquartile ranges with the whiskers and outliers with points.
725 Significance of Spearman rank correlations were assessed through asymptotic t approximation.
726 Differences in means between two groups with independent measures were tested using two-tailed t-
727 tests. When applicable, multiple testing was adjusted using Bonferroni correction for multiple
728 comparisons. A one-way ANOVA with 3 degrees of freedom was used in addition to two-tailed t-tests
729 in Fig. 6 to provide insights on overall versus group comparison. When analyzing datasets including
730 repeated measurements of the same individuals (Fig. 3a, Fig. 5b, Fig. 5c, Supplementary Fig. 8a,
731 Supplementary Fig. 10b), we used linear mixed models with time since positive RT-PCR or time since
732 symptom onset (continuous or binary variable) as fixed effect and individual as random effect. In the
733 case of Fig. 5c and Supplementary Fig. 10c, the decreasing slope of neutralization titers was estimated
734 by considering only individuals with neutralization titers above the detection levels (NT50>100) at their
735 first measurement. For all linear mixed models, a Wald test with two-sided hypothesis was used to
736 determine if the estimated slope was significantly different from 0. In addition, half-lives were
737 obtained from the decreasing slope estimated on the log of either MFI-FOEs (Fig. 5b, Supplementary
738 Fig. 10b) or NT50s (Fig. 5c, Supplementary Fig. 10c) as follows: t1/2=log(2)/(slope*log(10)). In Fig. 7b
739 and 7c, linear regressions were used to estimate the association between hCoV and SARS-CoV-2
740 reactivities: a Student t-test with two-sided hypothesis was used to assess if this association was
741 significantly different from 0.
742 **Data availability**

743 Serological measurements from all patients are made available in Supplementary Table 14.

744 **Code availability**

745 Codes to assess serostatus based on the ABCORA 2.3 method are available at:
746 https://github.com/chlpasin/SARS-CoV-2-serology

747 **References**

748

749 1 Rydyznski Moderbacher, C. *et al.* Antigen-Specific Adaptive Immunity to SARS-CoV-2 in Acute
750 COVID-19 and Associations with Age and Disease Severity. *Cell* **183**, 996-1012 e1019,
751 doi:10.1016/j.cell.2020.09.038 (2020).
752 2 Wheatley, A. K. *et al.* Evolution of immune responses to SARS-CoV-2 in mild-moderate COVID-
753 19. *Nature Communications* **12**, 1162, doi:10.1038/s41467-021-21444-5 (2021).
754 3 Wang, Z. *et al.* Enhanced SARS-CoV-2 neutralization by dimeric IgA. *Sci Transl Med* **13**,
755 doi:10.1126/scitranslmed.abf1555 (2021).
756 4 Robbiani, D. F. *et al.* Convergent antibody responses to SARS-CoV-2 in convalescent
757 individuals. *Nature* **584**, 437-442, doi:10.1038/s41586-020-2456-9 (2020).
758 5 Gaebler, C. *et al.* Evolution of antibody immunity to SARS-CoV-2. *Nature*, doi:10.1038/s41586-
759 021-03207-w (2021).
760 6 Muecksch, F. *et al.* Longitudinal analysis of serology and neutralizing antibody levels in
761 COVID19 convalescents. *J Infect Dis*, doi:10.1093/infdis/jiaa659 (2020).
762 7 Long, Q.-X. *et al.* Clinical and immunological assessment of asymptomatic SARS-CoV-2
763 infections. *Nature Medicine* **26**, 1200-1204, doi:10.1038/s41591-020-0965-6 (2020).
764 8 Robbiani, D. F. *et al.* Convergent antibody responses to SARS-CoV-2 in convalescent
765 individuals. *Nature* **584**, 437-442, doi:10.1038/s41586-020-2456-9 (2020).
766 9 Aziz, N. A. *et al.* Seroprevalence and correlates of SARS-CoV-2 neutralizing antibodies from a
767 population-based study in Bonn, Germany. *Nat Commun* **12**, 2117, doi:10.1038/s41467-021-
768 22351-5 (2021).
769 10 Fenwick, C. *et al.* Changes in SARS-CoV-2 Spike versus Nucleoprotein Antibody Responses
770 Impact the Estimates of Infections in Population-Based Seroprevalence Studies. *J Virol* **95**,
771 doi:10.1128/JVI.01828-20 (2021).
772 11 Buss, L. F. *et al.* Three-quarters attack rate of SARS-CoV-2 in the Brazilian Amazon during a
773 largely unmitigated epidemic. *Science* **371**, 288-292, doi:10.1126/science.abe9728 (2021).
774 12 Diagnostics, E. R. <https://diagnostics.roche.com/global/en/products/params/elecsys-anti-
775 sars-cov-2.html> (
776 13 Abbott. <https://www.corelaboratory.abbott/us/en/offerings/segments/infectious-
777 disease/sars-cov-2> (
778 14 Euroimmun. <https://www.euroimmun.com/products/infection-diagnostics/id/sars-cov-2-
779 infection-covid-19/> (
780 15 Pinto, D. *et al.* Cross-neutralization of SARS-CoV-2 by a human monoclonal SARS-CoV antibody.
781 *Nature* **583**, 290-295, doi:10.1038/s41586-020-2349-y (2020).
782 16 Piccoli, L. *et al.* Mapping Neutralizing and Immunodominant Sites on the SARS-CoV-2 Spike
783 Receptor-Binding Domain by Structure-Guided High-Resolution Serology. *Cell* **183**, 1024-
784 1042.e1021, doi:https://doi.org/10.1016/j.cell.2020.09.037 (2020).
785 17 Thomson, E. C. *et al.* Circulating SARS-CoV-2 spike N439K variants maintain fitness while
786 evading antibody-mediated immunity. *Cell* **184**, 1171-1187 e1120,
787 doi:10.1016/j.cell.2021.01.037 (2021).
788 18 Müller, L. *et al.* Sensitivity of anti-SARS-CoV-2 serological assays in a high-prevalence setting.
789 *European Journal of Clinical Microbiology & Infectious Diseases*, doi:10.1007/s10096-021-
790 04169-7 (2021).
791 19 Rogers, T. F. *et al.* Isolation of potent SARS-CoV-2 neutralizing antibodies and protection from
792 disease in a small animal model. *Science* **369**, 956-963, doi:10.1126/science.abc7520 (2020).
793 20 Barnes, C. O. *et al.* Structures of Human Antibodies Bound to SARS-CoV-2 Spike Reveal
794 Common Epitopes and Recurrent Features of Antibodies. *Cell* **182**, 828-842 e816,
795 doi:10.1016/j.cell.2020.06.025 (2020).

21 Starr, T. N. *et al.* Deep Mutational Scanning of SARS-CoV-2 Receptor Binding Domain Reveals Constraints on Folding and ACE2 Binding. *Cell* **182**, 1295-1310 e1220, doi:10.1016/j.cell.2020.08.012 (2020).
22 Weisblum, Y. *et al.* Escape from neutralizing antibodies by SARS-CoV-2 spike protein variants. *Elife* **9**, doi:10.7554/eLife.61312 (2020).
23 Zhang, S. F. *et al.* Epidemiology characteristics of human coronaviruses in patients with respiratory infection symptoms and phylogenetic analysis of HCoV-OC43 during 2010-2015 in Guangzhou. *PLoS One* **13**, e0191789, doi:10.1371/journal.pone.0191789 (2018).
24 van der Hoek, L. *et al.* Burden of disease due to human coronavirus NL63 infections and periodicity of infection. *Journal of Clinical Virology* **48**, 104-108, doi:https://doi.org/10.1016/j.jcv.2010.02.023 (2010).
25 Huang, A. T. *et al.* A systematic review of antibody mediated immunity to coronaviruses: kinetics, correlates of protection, and association with severity. *Nat Commun* **11**, 4704, doi:10.1038/s41467-020-18450-4 (2020).
26 Amanat, F. *et al.* A serological assay to detect SARS-CoV-2 seroconversion in humans. *Nat Med* **26**, 1033-1036, doi:10.1038/s41591-020-0913-5 (2020).
27 Ladner, J. T. *et al.* Epitope-resolved profiling of the SARS-CoV-2 antibody response identifies cross-reactivity with endemic human coronaviruses. *Cell Rep Med* **2**, 100189, doi:10.1016/j.xcrm.2020.100189 (2021).
28 *Diagnostic testing for SARS-CoV-2- Interim guidance*, <https://www.who.int/publications/i/item/diagnostic-testing-for-sars-cov-2> (
29 Ng, K. W. *et al.* Preexisting and de novo humoral immunity to SARS-CoV-2 in humans. *Science* **370**, 1339-1343, doi:10.1126/science.abe1107 (2020).
30 Francis, T. On the Doctrine of Original Antigenic Sin. *Proceedings of the American Philosophical Society* **104**, 572-578 (1960).
31 NIBSC.org. <https://www.nibsc.org/products/brm_product_catalogue/detail_page.aspx?catid=20/136> (
32 Schmidt, F. *et al.* Measuring SARS-CoV-2 neutralizing antibody activity using pseudotyped and chimeric viruses. *bioRxiv*, doi:10.1101/2020.06.08.140871 (2020).
33 Pinto, D. *et al.* Cross-neutralization of SARS-CoV-2 by a human monoclonal SARS-CoV antibody. *Nature* **583**, 290-295, doi:10.1038/s41586-020-2349-y (2020).
34 Brouwer, P. J. M. *et al.* Potent neutralizing antibodies from COVID-19 patients define multiple targets of vulnerability. *Science* **369**, 643-650, doi:10.1126/science.abc5902 (2020).
35 Wu, Y. *et al.* A noncompeting pair of human neutralizing antibodies block COVID-19 virus binding to its receptor ACE2. *Science* **368**, 1274-1278, doi:10.1126/science.abc2241 (2020).
36 Chi, X. *et al.* A neutralizing human antibody binds to the N-terminal domain of the Spike protein of SARS-CoV-2. *Science* **369**, 650-655, doi:10.1126/science.abc6952 (2020).
37 Yuan, M. *et al.* A highly conserved cryptic epitope in the receptor binding domains of SARS-CoV-2 and SARS-CoV. *Science* **368**, 630-633, doi:10.1126/science.abb7269 (2020).
38 FDA. Decisional Memorandum - Neutralization titer. (2020).
39 Schwarz, G. Estimating the Dimension of a Model. *The Annals of Statistics* **6**, 461-464, 464 (1978).
40 Nickbakhsh, S. *et al.* Epidemiology of Seasonal Coronaviruses: Establishing the Context for the Emergence of Coronavirus Disease 2019. *J Infect Dis* **222**, 17-25, doi:10.1093/infdis/jiaa185 (2020).
41 Lepiller, Q. *et al.* High incidence but low burden of coronaviruses and preferential associations between respiratory viruses. *J Clin Microbiol* **51**, 3039-3046, doi:10.1128/jcm.01078-13 (2013).
42 Zurich, C. o. *Numbers and facts on COVID-19 [Kanton Zürich. Zahlen & Fakten zu COVID-19]*, < https://www.zh.ch/de/gesundheit/coronavirus/zahlen-fakten-covid-19.html?keyword=covid19#/home (accessed mar 30, 2021)> (

43 Bartsch, Y. C. *et al.* Discrete SARS-CoV-2 antibody titers track with functional humoral stability. *Nat Commun* **12**, 1018, doi:10.1038/s41467-021-21336-8 (2021).
44 Stephenson, K. E. *et al.* Immunogenicity of the Ad26.COV2.S Vaccine for COVID-19. *JAMA*, doi:10.1001/jama.2021.3645 (2021).
45 Alter, G. *et al.* Collaboration between the Fab and Fc contribute to maximal protection against SARS-CoV-2 following NVX-CoV2373 subunit vaccine with Matrix-M vaccination. *Res Sq*, doi:10.21203/rs.3.rs-200342/v1 (2021).
46 Garcia-Beltran, W. F. *et al.* Multiple SARS-CoV-2 variants escape neutralization by vaccine-induced humoral immunity. *Cell*, doi:10.1016/j.cell.2021.03.013 (2021).
47 Wibmer, C. K. *et al.* SARS-CoV-2 501Y.V2 escapes neutralization by South African COVID-19 donor plasma. *Nat Med*, doi:10.1038/s41591-021-01285-x (2021).
48 Stamatatos, L. *et al.* mRNA vaccination boosts cross-variant neutralizing antibodies elicited by SARS-CoV-2 infection. *Science*, doi:10.1126/science.abg9175 (2021).
49 Planas, D. *et al.* Sensitivity of infectious SARS-CoV-2 B.1.1.7 and B.1.351 variants to neutralizing antibodies. *Nat Med*, doi:10.1038/s41591-021-01318-5 (2021).
50 Moyo-Gwete, T. *et al.* SARS-CoV-2 501Y.V2 (B.1.351) elicits cross-reactive neutralizing antibodies. *bioRxiv*, doi:10.1101/2021.03.06.434193 (2021).
51 Li, Q. *et al.* SARS-CoV-2 501Y.V2 variants lack higher infectivity but do have immune escape. *Cell*, doi:10.1016/j.cell.2021.02.042 (2021).
52 Wu, J. *et al.* SARS-CoV-2 infection induces sustained humoral immune responses in convalescent patients following symptomatic COVID-19. *Nat Commun* **12**, 1813, doi:10.1038/s41467-021-22034-1 (2021).
53 Ding, S. *et al.* Antibody Binding to SARS-CoV-2 S Glycoprotein Correlates with but Does Not Predict Neutralization. *Viruses* **12**, doi:10.3390/v12111214 (2020).
54 Iyer, A. S. *et al.* Persistence and decay of human antibody responses to the receptor binding domain of SARS-CoV-2 spike protein in COVID-19 patients. *Sci Immunol* **5**, doi:10.1126/sciimmunol.abe0367 (2020).
55 Jiang, X. L. *et al.* Lasting antibody and T cell responses to SARS-CoV-2 in COVID-19 patients three months after infection. *Nat Commun* **12**, 897, doi:10.1038/s41467-021-21155-x (2021).
56 Breton, G. *et al.* Persistent cellular immunity to SARS-CoV-2 infection. *J Exp Med* **218**, doi:10.1084/jem.20202515 (2021).
57 Dan, J. M. *et al.* Immunological memory to SARS-CoV-2 assessed for up to 8 months after infection. *Science* **371**, doi:10.1126/science.abf4063 (2021).
58 Song, G. *et al.* Cross-reactive serum and memory B cell responses to spike protein in SARS-CoV-2 and endemic coronavirus infection. *bioRxiv*, doi:10.1101/2020.09.22.308965 (2020).
59 Anderson, E. M. *et al.* Seasonal human coronavirus antibodies are boosted upon SARS-CoV-2 infection but not associated with protection. *Cell*, doi:10.1016/j.cell.2021.02.010 (2021).
60 Marot, S. *et al.* Rapid decline of neutralizing antibodies against SARS-CoV-2 among infected healthcare workers. *Nature Communications* **12**, 844, doi:10.1038/s41467-021-21111-9 (2021).
61 Wei, X. *et al.* Emergence of Resistant Human Immunodeficiency Virus Type 1 in Patients Receiving Fusion Inhibitor (T-20) Monotherapy. *Antimicrobial Agents and Chemotherapy* **46**, 1896-1905, doi:10.1128/aac.46.6.1896-1905.2002 (2002).
62 Liechti, T. *et al.* Development of a high-throughput bead based assay system to measure HIV-1 specific immune signatures in clinical samples. *J Immunol Methods* **454**, 48-58, doi:10.1016/j.jim.2017.12.003 (2018).
63 Breiman, L. Random Forests. *Machine Learning* **45**, 5-32, doi:10.1023/A:1010933404324 (2001).
64 Liaw, A. a. W., Matthew. Classification and Regression by randomForest. *R News* (2002).
65 Team, R. C. (R Foundation for Statistical Computing, Vienna, Austria, 2020).
66 Wright, M. N. & Ziegler, A. ranger: A Fast Implementation of Random Forests for High Dimensional Data in C++ and R. *2017* **77**, 17, doi:10.18637/jss.v077.i01 (2017).

67 <https://github.com/chlpasin/SARS-CoV-2-serology> (
68 Bates, D., Mächler, M., Bolker, B. & Walker, S. Fitting Linear Mixed-Effects Models Using lme4. *Journal of Statistical Software* **067** (2015).
69 Kuznetsova, A., Brockhoff, P. B. & Christensen, R. H. B. lmerTest Package: Tests in Linear Mixed Effects Models. *2017* **82**, 26, doi:10.18637/jss.v082.i13 (2017).
70 Wickham, H. *ggplot2: Elegant Graphics for Data Analysis*. (2016).

Funding

This work was supported by a grant of the Pandemiefonds of the University of Zurich Foundation to A.T., a grant of the Swiss Red Cross to B.F. and A.T., a grant of the University Hospital Zurich Innovation Grant to M.G.M., the Swiss National Science Foundation grant 31CA30_196906 to H.F.G., A.T., R.K. and the Gilead COVID-19 RFP Research Program COMMIT Grant #: IN-SW-983-6078 (to H.F.G., A.T., R.K.). I.A.A. is supported by a research grant of the Promedica Foundation. Roche Diagnostics supported the study with providing test material for a proportion of the Elecsys S tests.

Acknowledgments

We thank the staff of the Institute of Medical Virology diagnostics unit, sample triage and administration for their support and the staff of the participating clinics for coordinating the sample collection in the frame of the included clinical trials.

Author Contributions

I.A.A., C.P., M.S., A.T., H.F.G. and R.D.K. conceived and designed the study and analyzed data. I.A.A., M.S., M.M.S., S.E., M.C.H., L.M., M.E.S., A.H., A.A., C.R.N., J.B., M.H. designed and performed binding antibody experiments. P.R., J.W. and S.E. conducted neutralization experiments and analyzed data. S.S. developed an analysis app. C.P. and R.D.K. analyzed data. D.L.B., M.M., A.W., S.K.R., B.M.F., E.S., J.G., C.B., P.M.M.S., M.G.M., H.F.G., A.W., U.K., J.B. and M.H. were involved in patient recruitment, provided

926 samples from study and diagnostic repositories and analyzed patient data. A.T., I.A.A., C.P. and M.S.
927 wrote the manuscript, which all co-authors commented on.
928
929 **Declaration of interests**
930 The authors declare no competing financial interests.
931

932 **Figure legends**

933 **Fig. 1. Seroprofiling SARS-CoV-2 responses.** (a) Assessment of the multiplex SARS-CoV-2 ABCORA 2.0
934 on the indicated training (N= 823) and validation (N= 635) cohorts (Supplementary Table 3). Depicted
935 are MFI signals normalized to empty bead controls (MFI-FOE). Grey boxes indicate values above the
936 individually set MFI-FOE cut-offs for SARS-CoV-2 specific responses for each antigen (see
937 Supplementary Table 4). (b) Heatmap representing the measured MFI-FOE values and the outcomes
938 predicted with ABCORA 2.0 - 2.3 of training and validation cohort measurements shown in (a).
939 Negative, Positive, and Positive, partial refer to ranking according to ABCORA 2.0 as specified in
940 Supplementary Table 5. (c) Sensitivity and specificity of ABCORA 2 assay versions based on the
941 combined training and validation cohort data depicted in (a). Proportion of false negative samples
942 (sensitivity; green) and proportion of false positive samples (specificity; blue) are represented by the
943 reduction from 100% (outer circle) per segment. (d) Assessment of ABCORA 2.0 with the National
944 Institute for Biological Standards and Control (NIBSC) Anti SARS-CoV-2 Verification Panel (20/B770)
945 comprising SARS-CoV-2 positive (red) and negative (blue) panel serum samples. Grey boxes indicate
946 values above the ABCORA 2.0 MFI-FOE cut-offs for SARS-CoV-2 specific responses for individual
947 antigen-Ig combinations.

948 **Fig. 2. Quantification of SARS-CoV-2 specific antibody responses.** (a-c) Titrated plasma from SARS-
949 CoV-2 positive adults (N=72) were measured with ABCORA 2.0 and (a) 50% effective concentrations
950 (EC50; expressed as reciprocal plasma dilution) and (b) area under the curve values (AUC; expressed
951 as MFI) were calculated. (c) Titrated SARS-CoV-2 RBD and S1 responses were quantified using the RBD
952 specific monoclonal antibody CR3022 (produced as IgG, IgA and IgM; expressed as ng/ml) as external

953 standard. See Supplementary Fig.7 for additional quantification with the WHO International Standard
954 Anti-SARS-CoV-2 Immunoglobulin. (d) Spearman correlation matrix assessing agreement between
955 ABCORA 2.0 based quantification readouts (EC50, AUC, RBD Ab standardized), the basic MFI-FOE
956 measured at 1/100 plasma dilution (log), indicated summed logMFI-FOE values (1/100 dilution), and
957 Roche Elecsys Anti-SARS-CoV-2 (S) assay results (U/ml). Non-significant correlations are left blank.
958 Levels of significance are assessed by asymptotic t approximation of Spearman's rank correlation, and
959 corrected by the Bonferroni method for multiple testing ($p<0.05/780$). Color shading denotes
960 correlation coefficient.

961 **Fig. 3. Binding and neutralization activity are closely linked in early and late infection** (a) 50%
962 Neutralization titers (NT50) titers against Wuhan-Hu-1 pseudotype post SARS-CoV-2 infection in
963 patients with known positive SARS-CoV-2 RT-PCR date (N= 369). Patients were stratified according to
964 time since first diagnosis to investigate early (less than 30 days post RT-PCR, lavender) and late (more
965 than 30 days post RT-PCR, turquoise) neutralization responses. Difference between these two groups
966 was assessed with a linear mixed model with time since RT-PCR (binary variable early/late) as fixed
967 effect and individual as random effect and using a Wald test on the parameter associated with time
968 since RT-PCR (***: $p<0.001$). (b) Linear regression analysis to define association between neutralization
969 (reciprocal NT50) and antibody binding (MFI-FOE). Black lines indicate linear regression predictions
970 and grey shaded areas correspond to the 95% confidence intervals. Results depict early (lavender), late
971 (turquoise) and full cohort (black). n.s. denotes non-significant results. Levels of significance are
972 assessed by asymptotic t approximation of Spearman's rank correlation, and corrected by the
973 Bonferroni method for multiple testing ($p<0.05/1200$, see Supplementary Figures 8b and 9).

974 **Fig. 4. Predicting neutralization capacity as a function of binding activity.** (a) SARS-CoV-2 positive
975 donors (N=467) were stratified into high neutralizers (NT50 >250, N=332; blue) and no/low neutralizers
976 (NT50 <250, N=135; grey), based on their neutralization activity against Wuhan-Hu-1. (b) and (c)
977 Comparison of the prediction ability of six different classification models using 100 cross-validation
978 sets (divided as 80% for training and 20% for validation. (b) Comparison of models by area under the

979 curve (AUC). Each dot corresponds to one cross-validation set. (c) Bayesian information criterion (BIC)
980 of the five models based on logistic regression. The different models are: Univariable logistic
981 regressions (ULR). ULR-RBD: mean of MFI-FOE RBD. ULR-S1: mean of MFI-FOE S1. Multivariable logistic
982 regression (MLR). MLR-S1, RBD: mean of S1 reactivity and mean of RBD reactivity. MLR-PCA2 and MLR-
983 PCA4: MLR of 2 and 4 first axis of PCA analysis, respectively. PCA was based on all 12 SARS-CoV-2
984 antibody reactivities measured by ABCORA 2.0. Random forest (RF) including all antibody reactivities
985 measured by ABCORA 2.0. (d) ULR-S1 estimated ROC curve based on full data set (N=467). (e)
986 Measured NT50 value versus probability of NT50 >250 as predicted by ULR-S1 in five randomly chosen
987 validation sets (each symbol corresponds to a validation set). Purple colored symbols indicate a higher
988 than 0.70 probability of the respective sample to be neutralizing at NT50 >250 and are therefore
989 denoted as high neutralizers. Grey indicates samples with predicted neutralization NT50 <250,
990 therefore classified as no/low neutralizers. (f) Neutralization prediction based on a modified ULR-S1
991 model utilizing the diagnostic readout SOC instead of MFI-FOE values as input. Measured NT50 value
992 versus sum of S1 SOC values (IgG, IgA, IgM) are depicted. Dashed lines correspond to a NT50=250
993 horizontally and the sum S1 SOCs=9.7 vertically. The sum S1 SOCs=9.7 corresponds to the thresholds
994 depicted for ULR-S1 in (d) and (e). The grey shaded area corresponds to true positives (individuals with
995 NT50 >250 predicted as high neutralizers).

996 **Fig. 5. Monitoring temporal evolution of antibody responses.** (a) ABCORA 2.3 definition of
997 seropositivity in donors with positive RT-PCR confirmed SARS-CoV-2 infection and known RT-PCR date
998 (N=369). Seropositivity rating in relation to plasma sampling time point post diagnosis is depicted. Grey
999 shaded area highlights the first seven days since positive RT-PCR detection. (b) Linear mixed model,
1000 with time since RT-PCR as fixed effect and individual as random effect, estimating the decay of antibody
1001 binding activity based on ABCORA 2.0 measurements at 1 - 4 longitudinal time points in 120 individuals
1002 totaling in 251 measurements. Purple lines correspond to the models estimation and purple shaded
1003 areas to the 95% confidence intervals. Antibody half-lives (t1/2 in days) from significant models are
1004 depicted. Significance was assessed using Wald tests on the slope parameters. (c) Linear mixed model,

1005 with time since RT-PCR as fixed effect and individual as random effect, estimating the decay of
1006 neutralizing capacity on 251 measurements from 120 individuals. Only individuals with NT50>100 at
1007 their first measurement were used to estimate the half-life. The purple line corresponds to the model
1008 estimation and the purple shaded area to the 95% confidence intervals. Significance was assessed
1009 using Wald tests on the slope parameters.

1010 **Fig. 6. Seasonal and annual fluctuation in HCoV reactivity.** Reactivity to human coronaviruses (HCoV-
1011 NL63, HCoV-229E, HCoV-HKU1, HCoV-OC43) was compared by ABCORA 5.0. Reactivity in healthy blood
1012 donors from 2019 and 2020 was compared. Pre-pandemic samples included: January 2019 (N=285),
1013 May 2019 (N=288), January 2020 (N=252). Samples from May 2020 (N=672) were collected during the
1014 pandemic in Switzerland. Only samples without SARS-CoV-2 specific reactivity as defined by ABCORA
1015 were included (N=653). Stars correspond to levels of significance of two-tailed t-tests comparing the
1016 indicated groups. Levels of significance are corrected by the Bonferroni method for multiple testing
1017 and indicated as follows: *p<0.05/36, **p<0.01/36, ***p<0.001/36.

1018 **Fig. 7. Association between SARS-CoV-2 and HCoV antibody responses.** (a-b) Time-matched
1019 comparison of ABCORA 5.0 reactivity for SARS-CoV-2 (a) and HCoVs (b) in healthy and SARS-CoV-2
1020 infected individuals. Healthy donors were sampled in May 2020 (N=653; blue). Plasma from SARS-CoV-
1021 2 infected individuals were collected between April - June 2020 (N=65; red). See Supplementary Fig.
1022 13 for analysis on the full SARS-CoV-2 positive cohort (N=389). Grey boxes indicate values above the
1023 individual MFI-FOE cut-offs for SARS-CoV-2 specific responses for each antigen. Stars correspond to
1024 levels of significance of t-tests comparing negative versus positive patients. Levels of significance are
1025 corrected by the Bonferroni method for multiple testing and indicated as follows: *p<0.05/12,
1026 **p<0.01/12, ***p< 0.001/12. (b) Linear regression models showing the association between SARS-
1027 CoV-2 and HCoV signals in 204 SARS-CoV-2 positive patients with known dates of first positive RT-PCR
1028 detection. Influences within the same antibody class are investigated. The models were adjusted on
1029 age (spline with 3 degrees of freedom), gender, time since positive RT-PCR (spline with 3 degrees of
1030 freedom) and level of HCoV reactivity. Samples are defined to harbor high HCoV reactivity if they show

1031 ABCORA 5.0 HCoV logMFI-FOE values higher than the corresponding median in at least 3 HCoV
1032 measurements (HKU1, OC43, NL63 or 229E). Curves correspond to the models estimation and shaded
1033 areas to the 95% confidence intervals. p-values were obtained by running a Student t-test on the
1034 parameter associated to HCoV reactivity in the linear regression. (c) Linear regression model showing
1035 the association between SARS-CoV-2 IgG and HCoV IgA signals. Curves correspond to the models
1036 estimation and shaded areas to the 95% confidence intervals. (d) Linear regression model showing the
1037 association between SARS-CoV-2 IgG and HCoV IgM signals. Curves correspond to the models
1038 estimation and shaded areas to the 95% confidence intervals.

1039

1040 **Supplementary Figures**

1041 **Supplementary Fig.1. Schematic overview of ABCORA seroprofiling.** (a) Directed coupling of His-
1042 tagged antigens to magnetic beads covalently coupled with anti-His antibody. (b) Binding of patient
1043 plasma antibodies to antigen-coupled beads and detection by PE-labeled secondary antibodies (IgG,
1044 IgA or IgM) with the FlexMap 3D reader (Luminex). Median fluorescence intensity (MFI) proportional
1045 to bound secondary antibody is recorded. Figure created with BioRender.

1046 **Supplementary Fig. 2. Determination of optimal concentration of anti-His antibodies and SARS-CoV-**
1047 **2 derived antigens for coupling and loading of magnetic beads.** (a) Titration of anti-His capture
1048 antibody on magnetic beads. One of two independent experiments is depicted. (b) and (c) Optimization
1049 of antigen loading. (b) Reactivity of beads loaded with increasing doses of SARS-CoV-2 nucleoprotein
1050 (N) or SARS-CoV-2 spike protein subunit S1 (S1) with titered anti-N and anti-S1 mAbs and a SARS-CoV-
1051 2 positive patient plasma pool. One of three independent experiments is depicted. (c) Median
1052 fluorescence intensity (MFI) at 1/100 dilution and the 50 % effective concentration (EC50) values for
1053 anti-N and anti-S1 mAbs, the SARS-CoV-2 positive patient pool (+PP), two individual SARS-CoV-2
1054 positive patient plasma (P1 and P2) and a plasma pool of pre-pandemic healthy donors (-PP). One of
1055 three independent experiments is depicted. (d) Final assessment of assay setup (5 µg anti-his Ab per

1056 million beads, 320 nM His-tagged antigens, Phycoerythrin (PE)-labeled secondary antibodies at 17500).
1057 Reactivity of the indicated SARS-CoV-2 antigens with serial dilutions of anti-N and anti-S mAbs, positive
1058 and negative donor plasma pools was probed. Three independent experiments are depicted.

1059 **Supplementary Fig. 3. Assessment of assay variability.** Titration of the positive control plasma donor
1060 pool composed of 20 SARS-CoV-2 RT-PCR positive patients. Median fluorescence intensity (MFI) for
1061 IgG, IgA and IgM reactivities to SARS-CoV-2 proteins (RBD, S1, S2, N) and empty bead reactivity of 31
1062 independent titrations are shown.

1063 **Supplementary Fig. 4. Temporal stability and variability analysis**. (a) Assessment of the temporal
1064 stability of antigen coupled beads. The SARS-CoV-2 positive plasma pool was titrated on 25 days and
1065 the distribution of all signal intensities (pooled over plasma dilutions and antigens) for each day
1066 depicted. (b) Histogram of the overall assay variability (coefficient of variation) for all tested Ig classes
1067 based on the variability of mean log MFI values from 31 independent titrations (7 dilution steps) of the
1068 positive control plasma pool depicted in Supplementary Figure 3. (c-d) Boxplots depicting the overall
1069 assay variability stratified by the four different antigens (c) and plasma dilutions (d) based on 31
1070 independent titrations (7 dilution steps) of a positive plasma pool. (e) Boxplots showing the intraday
1071 variability stratified by the four different antigens based on six independent titrations of a positive
1072 plasma pool performed on the same day. (f) Boxplots showing the intra-day variability stratified by the
1073 four different antigens based on a titration of a positive plasma pool performed on 10 different days.

1074 **Supplementary Fig. 5. Interdependency of SARS-CoV-2 and HCoV HKU1 antibody reactivity.**
1075 Spearman correlation matrix of SARS-CoV-2 (RBD, S1, S2, N) and HKU1 S1 antigen reactivity (based on
1076 logMFI-FOE) in SARS-CoV-2 positive adults (N= 389), healthy, pre-pandemic adults (N=825), pre-
1077 pandemic samples from patients recently infected with a circulating HCoV strain (N=75) and pre-
1078 pandemic children (N=169). Non-significant correlations are left blank. Levels of significance are
1079 assessed by asymptotic t approximation of Spearman's rank correlation, and corrected by the
1080 Bonferroni method for multiple testing ($p<0.05/420$).

1081 **Supplementary Fig. 6. Variable importance for computational models.** (a) Correlation matrix of all
1082 immunoglobulin variables in SARS-CoV-2 positive patients from the training dataset (N=175). Defining
1083 five clusters based on hierarchical clustering showed that IgA N and IgM N clustered separately from
1084 other IgA and IgM variables. Other variables (indicated by stars: all IgGs, IgAs without N and IgMs
1085 without N) were highly correlated. We therefore used the mean of these three clusters in the logistic
1086 regression. (b) Variable importance (measured as the mean decrease of node impurity with Gini index).
1087 Each of the 100 dots corresponds to a random forest performed on a bootstrap sample of the training
1088 dataset (N=823).

1089 **Supplementary Fig. 7. Quantification of SARS-CoV-2 specific antibodies.** (a) Titration of SARS-CoV-2
1090 positive plasma pool used as plate standard curve for quantification in Figure 3 (N=72). Uncorrected
1091 MFI values are depicted. (b) Quantification of SARS-CoV-2 specific antibodies in the positive plasma
1092 pool by interpolating RBD and S1 content based on standard curves of the RBD-specific mAB CR3022
1093 (upper panel) or the WHO International Standard (lower panel). Data from three independent
1094 experiments are depicted. (c) Spearman correlation matrix assessing agreement between diverse
1095 ABCORA measurements and quantifications (individual and summed logMFI-FOE values at 1/100
1096 dilution of plasma, EC50, AUC, IU/ml content based on WHO Standard NIBSC 20/136) and Roche
1097 Elecsys Anti-SARS-CoV-2 (S) (U/ml). Non-significant correlations are left blank. Levels of significance
1098 are assessed by asymptotic t approximation of Spearman's rank correlation, and corrected by the
1099 Bonferroni method for multiple testing ($p<0.05/780$). Color shading denotes correlation coefficient.

1100 **Supplementary Fig. 8. Binding and neutralization activity are closely linked in early and late SARS-**
1101 **CoV-2 infection.** (a) 50% Neutralization titers (NT50) titers against Wuhan-Hu-1 pseudotype in patients
1102 with known date of symptoms onset (N= 333). Patients were stratified according to time since first
1103 diagnosis to investigate early (less than 30 days post symptoms onset, lavender) and late (more than
1104 30 days symptoms onset, turquoise) neutralization responses. Difference between these two groups
1105 was assessed with a linear mixed model with time since symptom onset (binary variable early/late) as
1106 fixed effect and individual as random effect and using a Wald test on the parameter associated with

1107 time since symptom onset (***p<0.001). (b) Linear regression analysis to define association between
1108 neutralization (reciprocal NT50) and antibody binding (MFI-FOE). Black lines indicate linear regression
1109 predictions. Levels of significance are assessed by asymptotic t approximation of Spearman's rank
1110 correlation, and corrected by the Bonferroni method for multiple testing (p<0.05/1200, see
1111 Supplementary Figure 9).

1112 **Supplementary Fig. 9. Correlation of antibody binding and neutralization activity in early and late**
1113 **infection**. Spearman correlation matrix assessing agreement between SARS-CoV-2 antigen reactivity
1114 (RBD, S1, S2, N) based on logMFI-FOE values and neutralization (NT50, NT80, NT90) in SARS-CoV-2
1115 positive adults (N= 389) divided in in early and late time points corresponding to time since positive
1116 RT-PCR diagnosis (a, N=118 – b, N=251) or symptom onset (c, N=66 – d, N=267). Non-significant
1117 correlations are left blank. Levels of significance are assessed by asymptotic t approximation of
1118 Spearman's rank correlation, and corrected by the Bonferroni method for multiple testing
1119 (p<0.05/1200).

1120 **Supplementary Fig. 10. Monitoring temporal evolution of antibody responses** (a) Heatmaps
1121 representing the measured MFI-FOE values and the outcome predicted with ABCORA 2.0 - 2.3 of
1122 measurements of SARS-CoV-2 positive patients with known dates of positive RT-PCR diagnosis (N=369)
1123 (upper panel) or with known dates of onset of symptoms (N=333) (lower panel). Purple and orange
1124 scales indicate days post positive RT-PCR or days post onset of symptoms, respectively, white-to-black
1125 scale indicates seroconversion predicted with the different ABCORA approaches. (b) Linear mixed
1126 model, with time since symptom onset as fixed effect and individual as random effect, estimating the
1127 decay of antibody binding activity based on ABCORA 2.0 measurements at 1-4 longitudinal time points
1128 in 120 individuals totaling in 251 measurements. Orange lines correspond to the models estimation
1129 and orange shaded areas to the 95% confidence intervals. Antibody half-lives (t1/2 in days) from
1130 significant models are depicted. Significance was assessed using Wald tests on the slope parameters.
1131 (c) Linear mixed model estimating the decay of neutralizing capacity in patients separated by their
1132 neutralizing activity. Only individuals with NT50>100 at their first measurement were used to estimate

1133 the half-life. The black line corresponds to the model estimation and the grey shaded area to the 95%
1134 confidence interval.

1135 **Supplementary Fig. 11. ABCORA 5 seroprofiling records antibody reactivity to SARS-CoV-2 and four**
1136 **HCoVs.** (a) Assessment of the multiplex SARS-CoV-2 ABCORA 5.0 on the indicated training (N= 825) and
1137 validation (N= 635) cohorts (Supplementary Table 3). Depicted are MFI signals normalized to empty
1138 bead controls (MFI-FOE). Grey boxes indicate values above the individually set MFI-FOE cut-offs for
1139 SARS-CoV-2 specific responses for each antigen (see Supplementary Table 4). (b) Sensitivity and
1140 specificity of ABCORA 5 assay versions 5.0, 5.4 and 5.5 based on the combined training and validation
1141 cohort data depicted in (a) (see also Supplementary Table 10). False negative proportion (sensitivity;
1142 green) and false positive proportion (specificity; blue) samples are represented by the reduction from
1143 100% (outer circle) per segment.

1144 **Supplementary Fig. 12. Interdependencies between antibody reactivity to SARS-CoV-2 and the four**
1145 **HCoVs.** Spearman correlation matrix assessing agreement between SARS-CoV-2 antigens (RBD, S1, S2,
1146 N) and HCoVs (229E, NL63, OC43, HKU1) (based on logMFI-FOE) in SARS-CoV-2 positive adults (N= 389),
1147 healthy, pre-pandemic adults (N= 825), pre-pandemic samples from patients recently infected with a
1148 circulating HCoV strain (N=75) and pre-pandemic children (N=169). Non-significant correlations are left
1149 blank. Levels of significance are assessed by asymptotic t approximation of Spearman's rank
1150 correlation, and corrected by the Bonferroni method for multiple testing ($p<0.05/1104$).

1151 **Supplementary Fig. 13. Association between SARS-CoV-2 and HCoV antibody responses.** Comparison
1152 of ABCORA 5.0 reactivity for SARS-CoV-2 and HCoVs in healthy, SARS-CoV-2 negative and SARS-CoV-2
1153 infected individuals. Healthy donors were sampled in May 2020 (N=653; blue). Plasma from SARS-CoV-
1154 2 infected individuals were collected between April 2020 and February 2021 (N=389; red, Training III
1155 and Validation VI). Grey boxes indicate values above the individual MFI-FOE cut-offs for SARS-CoV-2
1156 specific responses for each antigen. Stars correspond to levels of significance of two-tailed t-tests

1157 comparing negative versus positive patients. Levels of significance are corrected by the Bonferroni

1158 method for multiple testing and indicated as follows: *$p<0.05/12$, **$p<0.01/12$, ***$p< 0.001/12$.

1159

1160

Figure 1

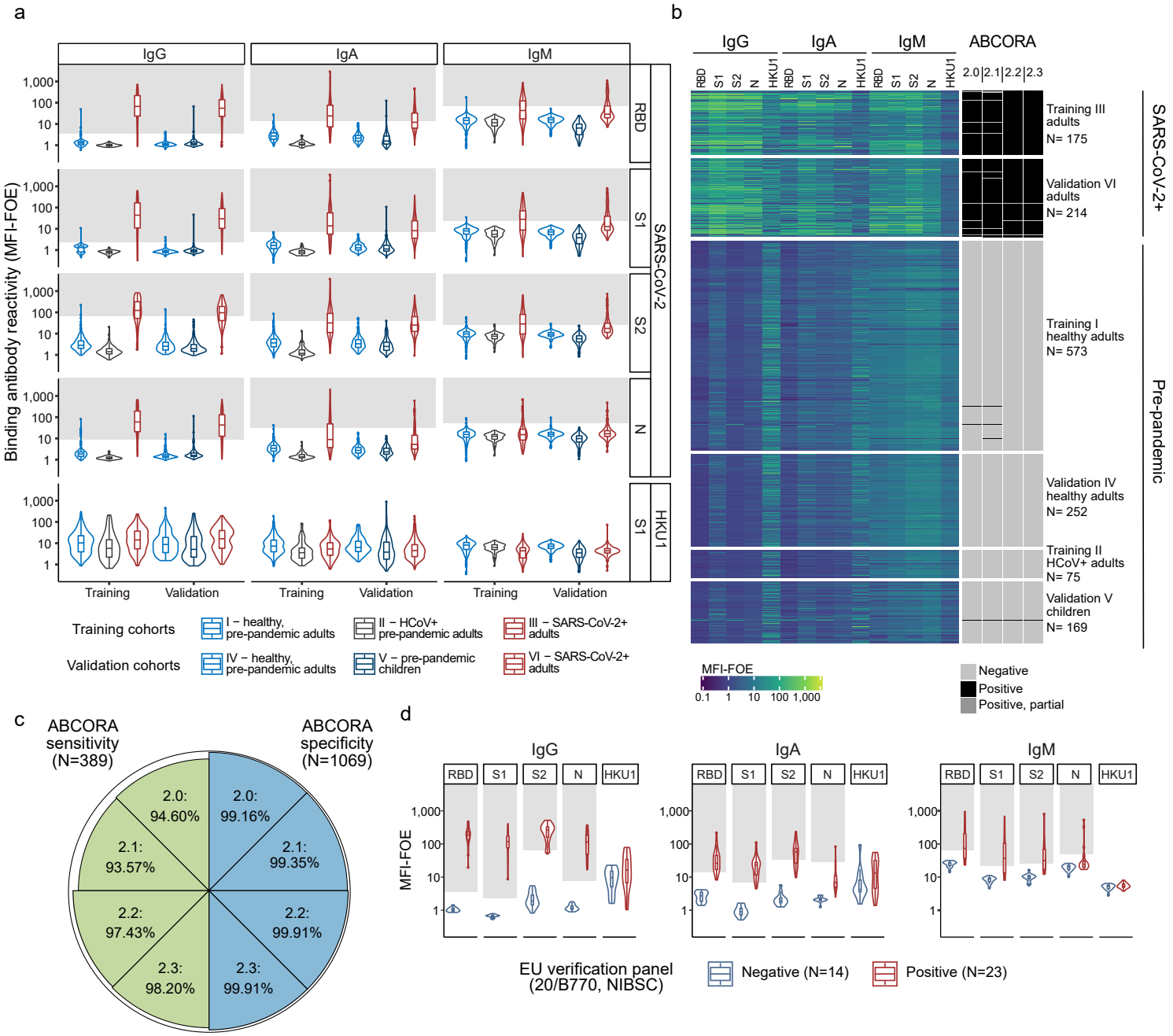

Fig 1. Seroprofiling SARS-CoV-2 responses. (a) Assessment of the multiplex SARS-CoV-2 ABCORA 2.0 on the indicated training (N= 823) and validation (N= 635) cohorts (Supplementary Table 3). Depicted are MFI signals normalized to empty bead controls (MFI-FOE). Grey boxes indicate values above the individually set MFI-FOE cut-offs for SARS-CoV-2 specific responses for each antigen (see Supplementary Table 4). (b) Heatmap representing the measured MFI-FOE values and the outcomes predicted with ABCORA 2.0 - 2.3 of training and validation cohort measurements shown in (a). Negative, Positive, Positive, partial refer to ranking according to ABCORA 2.0 as specified in Supplementary Table 5. (c) Sensitivity and specificity of ABCORA 2 assay versions based on the combined training and validation cohort data depicted in (a). Proportion of false negative samples (sensitivity; green) and proportion of false positive samples (specificity; blue) are represented by the reduction from 100% (outer circle) per segment. (d) Assessment of ABCORA 2 with the National Institute for Biological Standards and Control (NIBSC) Anti SARS-CoV-2 Verification Panel (20/B770) comprising SARS-CoV-2 positive (red) and negative (blue) panel serum samples. Grey boxes indicate values above the ABCORA 2.0 MFI-FOE cut-offs for SARS-CoV-2 specific responses for individual antigen-Ig combinations.

Figure 2

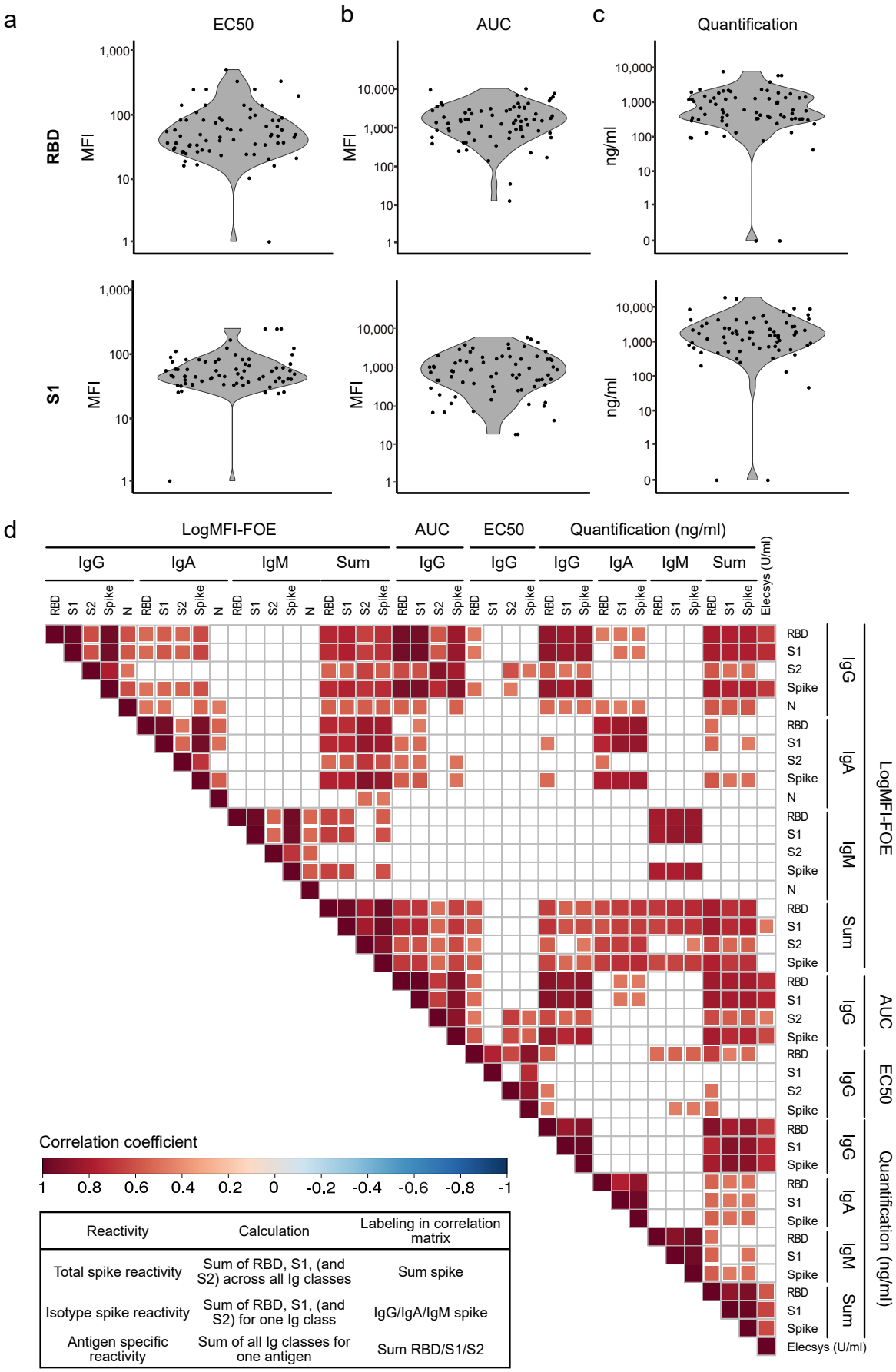

Reactivity	Calculation	Labeling in correlation matrix
Total spike reactivity	Sum of RBD, S1, (and S2) across all Ig classes	Sum spike
Isotype spike reactivity	Sum of RBD, S1, (and S2) for one Ig class	IgG/IgA/IgM spike
Antigen specific reactivity	Sum of all Ig classes for one antigen	Sum RBD/S1/S2

Fig 2. Quantification of SARS-CoV-2 specific antibody responses. (a-c) Titrated plasma from SARS-CoV-2 positive adults (N=72) were measured with ABCORA 2.0 and (a) 50% effective concentrations (EC50; expressed as reciprocal plasma dilution) and (b) area under the curve values (AUC; expressed as MFI) were calculated. (c) Titrated SARS-CoV-2 RBD and S1 responses were quantified using the RBD specific monoclonal antibody CR3022 (produced as IgG, IgA and IgM; expressed as ng/ml) as external standard. See Supplementary Fig.7 for additional quantification with the WHO International Standard Anti-SARS-CoV-2 Immunoglobulin. (d) Spearman correlation matrix assessing agreement between ABCORA 2.0 based quantification readouts (EC50, AUC, RBD Ab standardized), the basic MFI-FOE measured at 1/100 plasma dilution (log), indicated summed LogMFI-FOE values (1/100 dilution), and Roche Elecsys Anti-SARS-CoV-2 (S) assay results (U/ml). Non-significant correlations are left blank. Levels of significance are assessed by asymptotic t approximation of Spearman's rank correlation, and corrected by the Bonferroni method for multiple testing ($p<0.05/780$). Color shading denotes correlation coefficient.

Figure 3

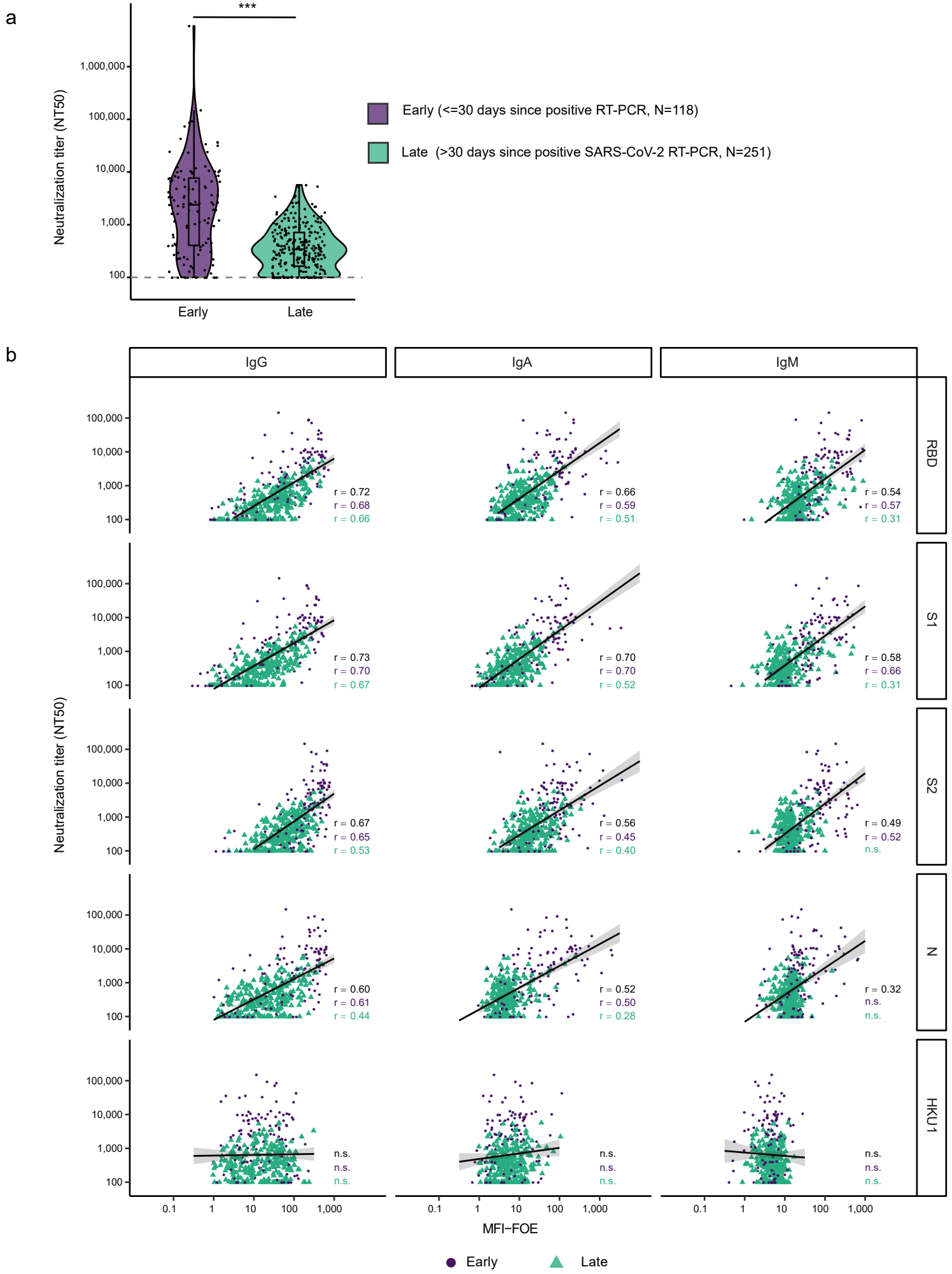
a
***
Neutralization titer (NT50)
1,000,000
100,000
10,000
1,000
100
Early
Late
Early (<=30 days since positive RT-PCR, N=118)
Late (>30 days since positive SARS-CoV-2 RT-PCR, N=251)
b
IgG
IgA
IgM
RBD
S1
S2
N
HKU1
r = 0.72
r = 0.68
r = 0.66
r = 0.66
r = 0.59
r = 0.51
r = 0.54
r = 0.57
r = 0.31
r = 0.73
r = 0.70
r = 0.67
r = 0.70
r = 0.70
r = 0.52
r = 0.58
r = 0.66
r = 0.31
r = 0.67
r = 0.65
r = 0.53
r = 0.56
r = 0.45
r = 0.40
r = 0.49
r = 0.52
n.s.
r = 0.60
r = 0.61
r = 0.44
r = 0.52
r = 0.50
r = 0.28
r = 0.32
n.s.
n.s.
n.s.
n.s.
n.s.
n.s.
n.s.
n.s.
n.s.
n.s.
n.s.
n.s.
0.1
1
10
100
1,000
MFI−FOE
Early
Late

Fig 3. Binding and neutralization activity are closely linked in early and late infection (a) 50% Neutralization titers (NT50) titers against Wuhan-Hu-1 pseudotype post SARS-CoV-2 infection in patients with known positive SARS-CoV-2 RT-PCR date (N= 369). Patients were stratified according to time since first diagnosis to investigate early (less than 30 days post RT-PCR, lavender) and late (more than 30 days post RT-PCR, turquoise) neutralization responses. Difference between these two groups was assessed with a linear mixed model with time since RT-PCR (binary variable early/late) as fixed effect and individual as random effect and using a Wald test on the parameter associated with time since RT-PCR (***: $p<0.001$). (b) Linear regression analysis to define association between neutralization (reciprocal NT50) and antibody binding (MFI-FOE). Black lines indicate linear regression predictions and grey shaded areas correspond to the 95% confidence intervals. Results depict early (lavender), late (turquoise) and full cohort (black). n.s. denotes non-significant results. Levels of significance are assessed by asymptotic t approximation of Spearman's rank correlation, and corrected by the Bonferroni method for multiple testing ($p<0.05/1200$, see Supplementary Figures 8b and 9).

Figure 4

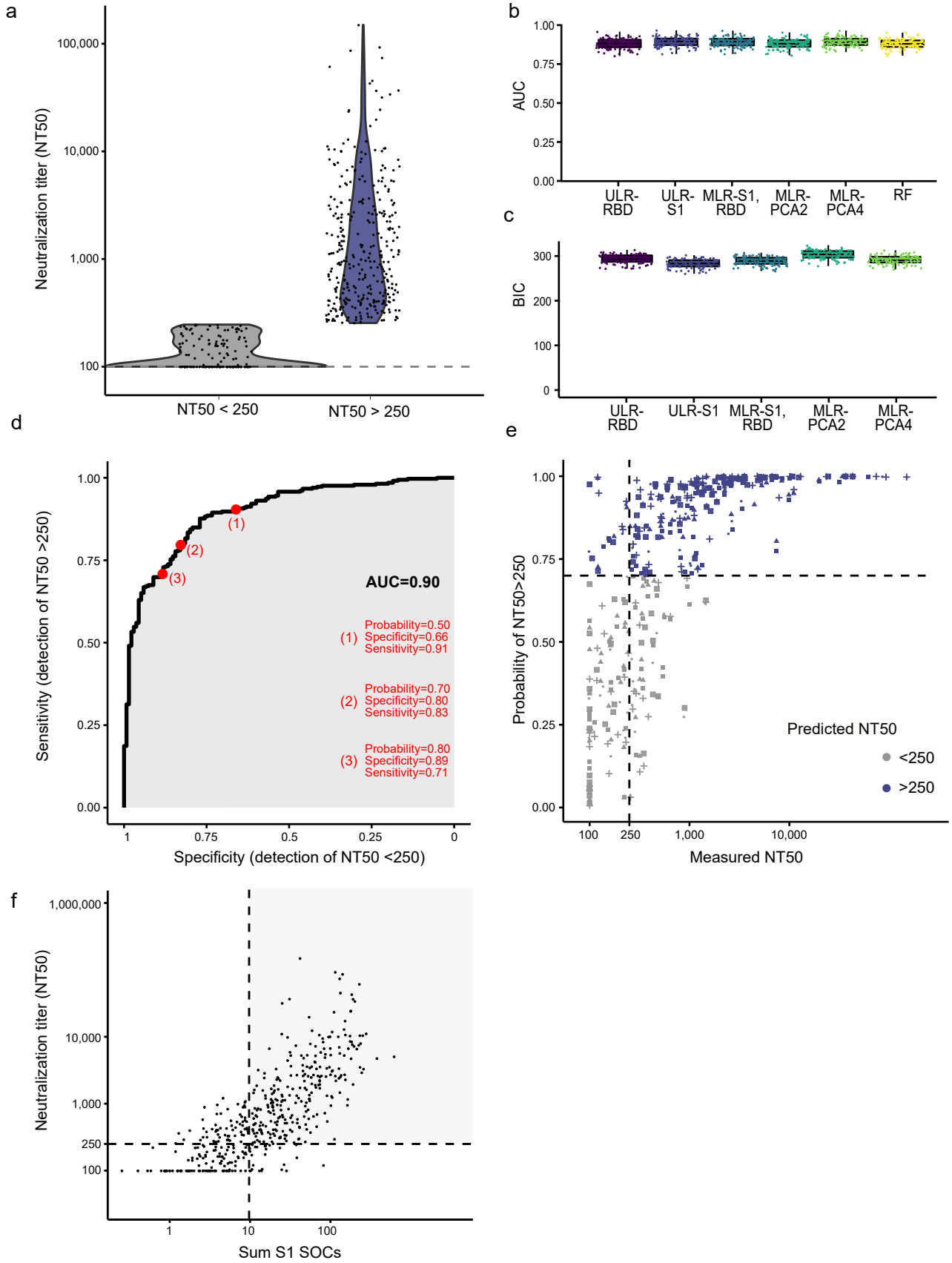

Fig 4. Predicting neutralization capacity as a function of binding activity. (a) SARS-CoV-2 positive donors (N=467) were stratified into high neutralizers (NT50>250, N=332; blue) and no/low neutralizers (NT50<250, N=135; grey), based on their neutralization activity against Wuhan-Hu-1. (b) and (c) Comparison of the prediction ability of six different classification models using 100 cross-validation sets (divided as 80% for training and 20% for validation. (b) Comparison of models by area under the curve (AUC). Each dot corresponds to one cross-validation set. (c) Bayesian information criterion (BIC) of the five models based on logistic regression. The different models are: Univariable logistic regressions (ULR). ULR-RBD: mean of MFI-FOE RBD. ULR-S1: mean of MFI-FOE S1. Multivariable logistic regression (MLR). MLR-S1, RBD: mean of S1 reactivity and mean of RBD reactivity. MLR-PCA2 and MLR-PCA4: MLR of 2 and 4 first axis of PCA analysis, respectively. PCA was based on all 12 SARS-CoV-2 antibody reactivities measured by ABCORA 2.0. Random forest (RF) including all antibody reactivities measured by ABCORA 2.0. (d) ULR-S1 estimated ROC curve based on full data set (N=467). (e) Measured NT50 value versus probability of NT50>250 as predicted by ULR-S1 in five randomly chosen validation sets (each symbol corresponds to a validation set). Purple colored symbols indicate a higher than 0.70 probability of the respective sample to be neutralizing at NT50>250 and are therefore denoted as high neutralizers. Grey indicates samples with predicted neutralization NT50<250, therefore classified as no/low neutralizers. (f) Neutralization prediction based on a modified ULR-S1 model utilizing the diagnostic readout SOC instead of MFI-FOE values as input. Measured NT50 value versus sum of S1 SOC values (IgG, IgA, IgM) are depicted. Dashed lines correspond to a NT50=250 horizontally and the sum S1 SOCs=9.7 vertically. The sum S1 SOCs=9.7 corresponds to the thresholds depicted for ULR-S1 in (d) and (e). The grey shaded area corresponds to true positives (individuals with NT50 >250 predicted as high neutralizers).

Figure 5

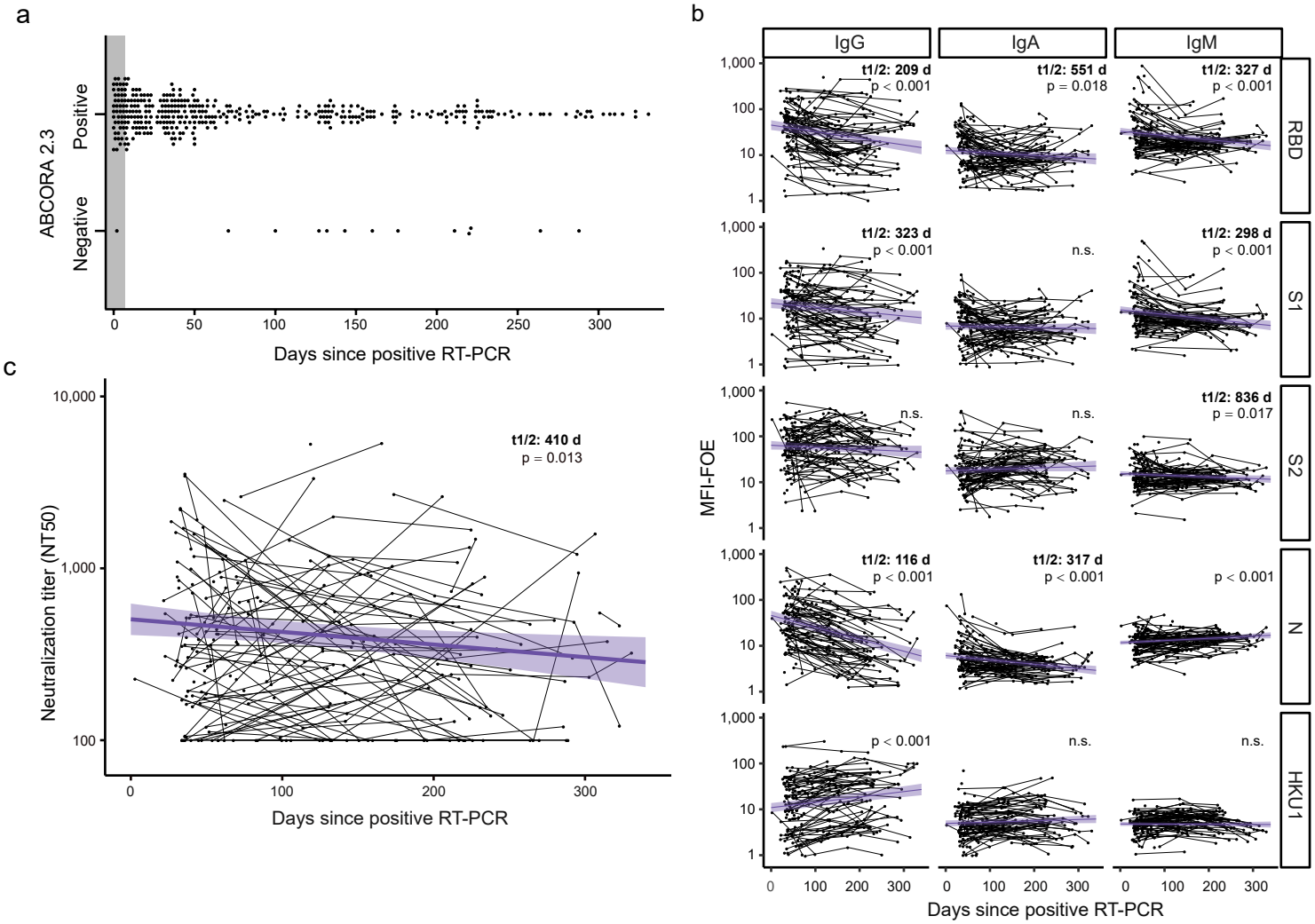

Fig 5. Monitoring temporal evolution of antibody responses(a) ABCORA 2.3 definition of seropositivity in donors with positive RT-PCR confirmed SARS-CoV-2 infection and known RT-PCR date (N=369). Seropositivity rating in relation to plasma sampling time point post diagnosis is depicted. Grey shaded area highlights the first seven days since positive RT-PCR detection. (b) Linear mixed model, with time since RT-PCR as fixed effect and individual as random effect, estimating the decay of antibody binding activity based on ABCORA 2.0 measurements at 1 - 4 longitudinal time points in 120 individuals totaling in 251 measurements. Purple lines correspond to the models estimation and purple shaded areas to the 95% confidence intervals. Antibody half-lives (t1/2 in days) from significant models are depicted. Significance was assessed using Wald tests on the slope parameters. (c) Linear mixed model, with time since RT-PCR as fixed effect and individual as random effect, estimating the decay of neutralizing capacity on 251 measurements from 120 individuals. Only individuals with NT50>100 at their first measurement were used to estimate the half-life. The purple line corresponds to the model estimation and the purple shaded area to the 95% confidence intervals. Significance was assessed using Wald tests on the slope parameters.

Figure 6

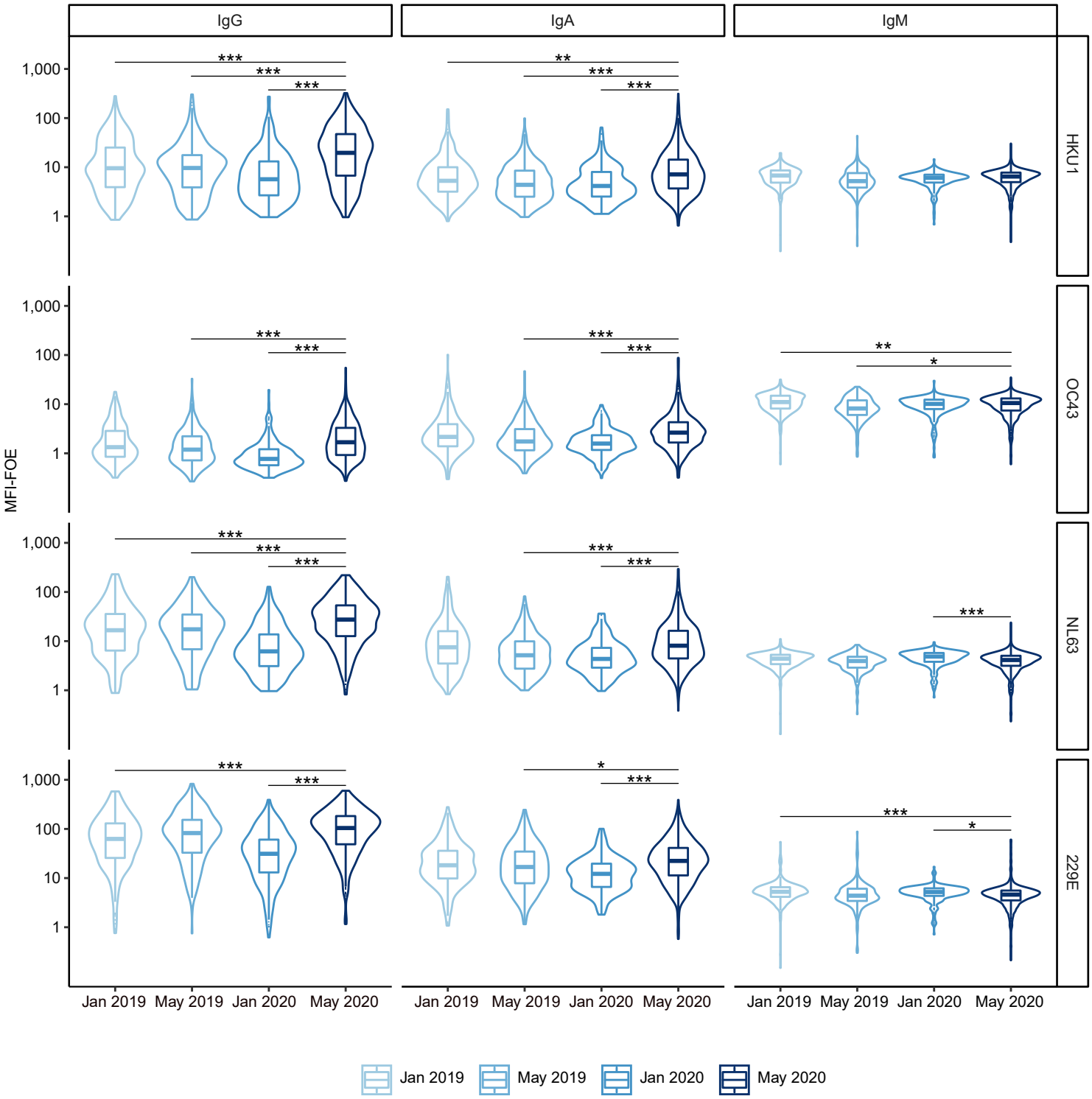

Fig 6. Seasonal and annual fluctuation in HCoV reactivity Reactivity to human coronaviruses (HCoV-NL63, HCoV-229E, HCoV-HKU1, HCoV-OC43) was compared by ABCORA 5.0. Reactivity in healthy blood donors from 2019 and 2020 was compared. Pre-pandemic samples included: January 2019 (N=285), May 2019 (N=288), January 2020 (N=252). Samples from May 2020 (N=672) were collected during the pandemic in Switzerland. Only samples without SARS-CoV-2 specific reactivity as defined by ABCORA were included (N=653). Stars correspond to levels of significance of two-tailed t-tests comparing the indicated groups. Levels of significance are corrected by the Bonferroni method for multiple testing and indicated as follows: *p<0.05/36, **p<0.01/36, ***p<0.001/36.

Figure 7

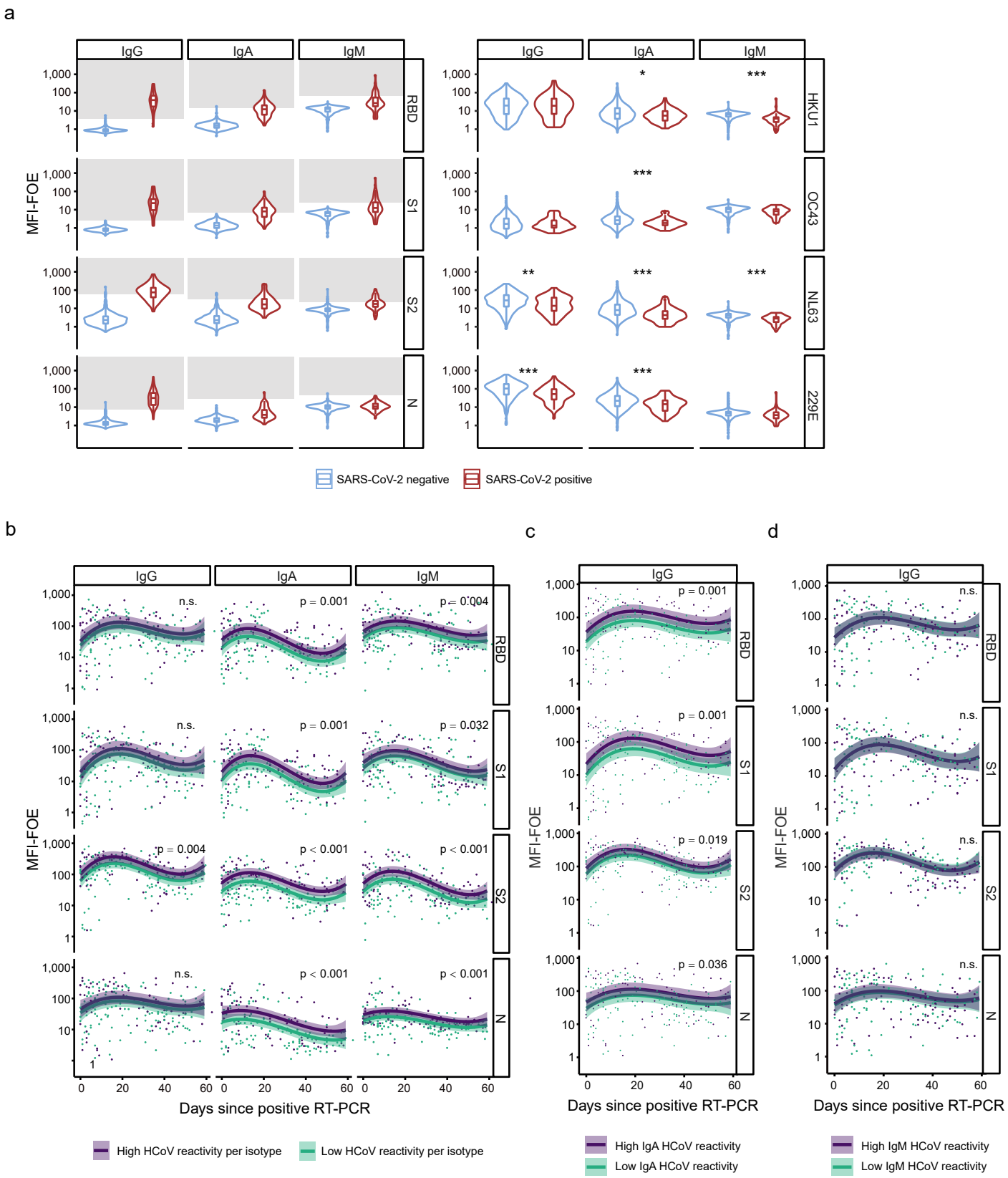

Fig 7. Association between SARS-CoV-2 and HCoV antibody responses. (a-b) Time-matched comparison of ABCORA 5.0 reactivity for SARS-CoV-2 (a) and HCoVs (b) in healthy and SARS-CoV-2 infected individuals. Healthy donors were sampled in May 2020 (N=653; blue). Plasma from SARS-CoV-2 infected individuals were collected between April - June 2020 (N=65; red). See Supplementary Figure 13 for analysis on the full SARS-CoV-2 positive cohort (N=389). Grey boxes indicate values above the individual MFI-FOE cut-offs for SARS-CoV-2 specific responses for each antigen. Stars correspond to levels of significance of t-tests comparing negative versus positive patients. Levels of significance are corrected by the Bonferroni method for multiple testing and indicated as follows: *p<0.05/12, **p<0.01/12, ***p< 0.001/12. (b) Linear regression models showing the association between SARS-CoV-2 and HCoV signals in 204 SARS-CoV-2 positive patients with known dates of first positive RT-PCR detection. Influences within the same antibody class are investigated. The models were adjusted on age (spline with 3 degrees of freedom), gender, time since positive RT-PCR (spline with 3 degrees of freedom) and level of HCoV reactivity. Samples are defined to harbor high HCoV reactivity if they show ABCORA 5.0 HCoV LogMFI-FOE values higher than the corresponding median in at least 3 HCoV measurements (HKU1, OC43, NL63 or 229E). Curves correspond to the models estimation and shaded areas to the 95% confidence intervals. p-values were obtained by running a Student t-test on the parameter associated to HCoV reactivity in the linear regression. (c) Linear regression model showing the association between SARS-CoV-2 IgG and HCoV IgA signals. Curves correspond to the models estimation and shaded areas to the 95% confidence intervals. (d) Linear regression model showing the association between SARS-CoV-2 IgG and HCoV IgM signals. Curves correspond to the models estimation and shaded areas to the 95% confidence intervals.